1	Convergent evolution of bacterial ceramide synthesis
2	Gabriele Stankeviciute ^{1,2} , Peijun Tang ³ , Ben Ashley ³ , Joshua D. Chamberlain ¹ , Matthew E.B.
3	Hansen ⁴ , Aimiyah Coleman ¹ , Rachel D'Emilia ¹ , Larina Fu ¹ , Eric C. Mohan ³ , Hung Nguyen ¹ ,
4	Ziqiang Guan ^{5,*} , Dominic J. Campopiano ^{3,*} , and Eric A. Klein ^{1,2,6,*} .
5	
6	Affiliations:
7	¹ Center for Computational and Integrative Biology, Rutgers University-Camden, Camden, NJ
8	08102, USA
9	² Rutgers Center for Lipid Research, Rutgers University, New Brunswick, NJ 08901, USA
10	³ East Chem School of Chemistry, University of Edinburgh, Edinburgh EH9 3FJ, United
11	Kingdom
12	⁴ Department of Genetics, Perelman School of Medicine at the University of Pennsylvania,
13	Philadelphia, PA 19104, USA
14	⁵ Department of Biochemistry, Duke University Medical Center, Durham, NC 27710, USA
15	⁶ Biology Department, Rutgers University-Camden, Camden, NJ 08102, USA.
16	*Correspondence to: eric.a.klein@rutgers.edu, Dominic.Campopiano@ed.ac.uk, and
17	ziqiang.guan@duke.edu
18	

Abstract: The bacterial domain produces numerous types of sphingolipids with various physiological functions. In the human microbiome, commensal and pathogenic bacteria use these lipids to modulate the host inflammatory system. Despite their growing importance, their biosynthetic pathway remains undefined since several key eukaryotic ceramide synthesis enzymes have no bacterial homologue. Here we used genomic and biochemical approaches to identify six proteins comprising the complete pathway for bacterial ceramide synthesis.

Bioinformatic analyses revealed the widespread potential for bacterial ceramide synthesis leading to our discovery of the first Gram-positive species to produce ceramides. Biochemical evidence demonstrated that the bacterial pathway operates in a different order than in eukaryotes. Furthermore, phylogenetic analyses support the hypothesis that the bacterial and eukaryotic ceramide pathways evolved independently.

Introduction

32

33

34

35

36

37

38

39

40

41

42

43

44

45

46

47

48

49

50

51

52

53

54

Sphingolipids are found ubiquitously in eukaryotes from fungi, to plants, to animals. By contrast, this class of lipids has been identified in only a handful of bacterial taxa¹. Within this small group of sphingolipid-producing bacteria there is a tremendous variety of acyl chain length and degree of saturation, acyl chain hydroxylation, and lipid headgroups. This structural diversity is paralleled by a wide range of physiological roles for sphingolipids including modulation of host-microbe interactions^{2,3}, protection from bacteriophage⁴, bacterial life cycle and sporulation⁵, and microbial predation⁶. Deeper investigations into the mechanistic roles of sphingolipids in bacterial physiology and host-microbe interactions have been hampered by a lack of knowledge of their biosynthetic pathway. Due to their importance in human health and disease⁷, it is not surprising that the eukaryotic biosynthesis pathway has been elucidated in tremendous detail⁸. By contrast, bacteria do not appear to have homologous enzymes, except for serine palmitoyltransferase (Spt) which performs the initial conserved step in ceramide synthesis^{9,10}. To date, the presence of predicted *spt* genes is the only indication that a bacterial species may synthesize sphingolipids¹¹. However, the presence of a predicted Spt alone is not a particularly reliable indicator of sphingolipid production because there is a high degree of similarity between members of the larger family of α-oxoamine synthases that are involved in heme and biotin synthesis. Here, we identified and characterized the remainder of the bacterial ceramide synthetic pathway. We note that during the preparation of this manuscript, the same set of genes were identified in C. crescentus¹². While the independent identification of this biosynthetic pathway corroborates the importance of these genes in ceramide synthesis, our

biochemical data suggested a different function for these enzymes than that originally

proposed¹². Furthermore, the elucidation of the bacterial ceramide synthesis pathway enabled us to perform a bioinformatic screen that led to the identification of 17 taxonomic classes, including the first Gram-positive bacteria, with the potential to synthesize sphingolipids. Lipid profiling of one of these Actinobacteria provided the first demonstration of Gram-positive bacterial ceramides, validated our bioinformatic approach, and suggested that bacterial sphingolipid synthesis occurs across a wide range of organisms. Surprisingly, the bacterial enzymes are not phylogenetically related to those in eukaryotes and the biosynthetic steps occur in a different order than in eukaryotes. These findings support the independent evolution of ceramide production in bacteria and eukaryotes.

Results

Characterization of serine palmitoyltransferase (Spt)

The first step in *de novo* ceramide synthesis, which is conserved between eukaryotes and prokaryotes, is the decarboxylative, Claisen-like condensation of palmitoyl-coenzyme A (palmitoyl-CoA) and L-serine into 3-ketosphinghanine (3-KDS, 1) (Fig. 1a)¹³. In *C. crescentus*, we previously identified $ccna_01220$ as a putative Spt since the $\Delta ccna_01220$ strain had no detectable ceramide⁴. His-tagged recombinant CCNA_01220 was purified from *E. coli* (see Extended Data Fig. 1a-b); it displayed Spt activity, and the production of 3-KDS was detected by matrix-assisted laser desorption ionization mass spectrometry (MALDI-MS) (Fig. 1b). Kinetic analyses yielded K_m values of 110.40 \pm 13.37 μ M and 2.98 \pm 0.25 mM for C16:0-CoA and L-serine, respectively (Fig. 1c), which are comparable to the values determined for *Sphingomonas paucimobilis* and human Spt¹⁴⁻¹⁶. *C. crescentus* Spt also condensed serine and C16:1-CoA with similar kinetic parameters (see Extended Data Fig. 1c-d). Liquid chromatography/electrospray

ionization-tandem mass spectrometry (LC/ESI-MS/MS) analysis of the ceramide molecule from C. crescentus showed that C16:0 was preferentially used as the Spt substrate to form the long-chain base (see Extended Data Fig. 1e). In some organisms, such as the gut commensal Bacteroides thetaiotaomicron, 1-deoxysphingolipids can be detected when Spt uses alanine as a substrate rather than serine². Similarly, a C. crescentus serine auxotroph ($\Delta serA$), produced 1-deoxyceramide (see Extended Data Fig. 1f-g).

Genetic screen identifies the ceramide synthesis pathway

In the absence of ceramides, *C. crescentus* becomes resistant to the cationic antimicrobial peptide, polymyxin B (PMX) and increasingly sensitive to bacteriophage Φcr30⁴. Using these two phenotypes of ceramide depletion, we performed a transposon mutagenesis screen incorporating both positive and negative selection to identify candidate genes involved in ceramide synthesis (see Extended Data Fig. 2A, detailed in Materials and Methods). Transposon insertions in cells displaying both selection phenotypes were mapped (see Supplementary Data Table 1 and Extended Data Fig. 2b) and multiple insertions were found in the *spt* gene validating this approach. These transposon mutants served as a platform for identifying ceramide synthesis enzymes as described below.

Spt enzymes vary in their preferred acyl-CoA substrate; some enzymes utilize fatty acyl-CoA thioesters whereas others use an acyl-chain bound as a thioester to an acyl carrier protein (ACP). Our genetic screening identified *ccna_01223*, a putative acyl-CoA synthetase, which adds CoA to a long-chain fatty acid. Additionally, inspection of neighboring genes revealed a candidate ACP (*ccna_01221*). This genomic arrangement of the Spt, ACP, and ACP-synthetase is similar to that seen in *Sphingomonas wittichii*¹⁷. Although no transposon insertions were

identified in *ccna_01221*, this was not surprising given that the gene is only 261 bp and would therefore have a low probability of containing an insertion. Deletion of either gene resulted in a total loss of ceramides (see Extended Data Fig. 3a-b) and both deletions could be complemented by ectopic expression of the respective gene (see Extended Data Fig. 3a-b). Total ion and extracted ion chromatograms confirm that the deletions did not disrupt global lipid production (see Extended Data Fig. 3c-d and Supplementary Table 3).

101

102

103

104

105

106

107

108

109

110

111

112

113

114

115

116

117

118

119

120

121

122

123

In eukaryotes, the second synthetic step is the reduction of 3-KDS to sphinganine (2), which is catalyzed by a NADPH-dependent 3-ketodihydrosphinghanine reductase (KDSR) (Fig. 1a). Among our transposon insertions, ccna 01222 was annotated as an NADH ubiquinoneoxidoreductase. Deletion of ccna 01222 resulted in a ceramide molecule with a mass reduction of 2 Da (Fig. 2a), corresponding to a loss of two hydrogens. Tandem mass spectrometry (MS/MS) analysis confirmed the retention of the oxidized double bond on the 3-KDS derived sphingoid base (see Extended Data Fig. 4). Complementation of the ccna 01222 deletion restored ceramide reduction (Fig. 2a). These data suggest that the bacterial reductase acts after the second acyl chain is added to 3-KDS. This contrasts with the eukaryotic pathway where deletion of KDSR generally leads to an accumulation of 3-KDS substrate and prevents downstream reactions¹⁸. There have been reports of 3-KDS being acylated directly by ceramide synthase in eukaryotic cells; however, this was only observed when Spt was highly overexpressed and cells were provided with excess serine and palmitate¹⁹. Since the bacterial reductase uses oxidized ceramide (oxCer) (6) as a substrate, we have named CCNA 01222 <u>Ceramide Reductase (CerR).</u>

In eukaryotes, the second acyl chain is attached to the sphingoid backbone by ceramide synthase (CerS) to form dihydroceramide (4) (Fig. 1a). Analysis of our transposon hits pointed to

ccna 01212 as a potential CerS. In C. crescentus, this gene is annotated as a dATP pyrophosphohydrolase; however, closely related genes identified by BLAST have a variety of annotations including Gcn5-related N-acetyltransferase (GNAT). Deletion of ccna 01212 led to a complete loss of ceramides (Fig. 2b), consistent with its role in ceramide synthesis. To confirm the enzymatic activity of CCNA 01212, recombinant protein purified from E. coli (see Extended Data Fig. 5a-b) was incubated with the substrates 3-KDS and palmitoyl-CoA. LC/ESI-MS/MS analysis of the reaction product identified the expected ceramide molecule (Fig. 2c). Kinetic analyses showed that CCNA 01212 constitutively hydrolyzed acyl-CoA even in the absence of 3-KDS, and the reaction exhibits substrate inhibition (see Extended Data Fig. 5c). Upon the addition of 3-KDS, the reaction proceeded according to Michaelis-Menten kinetics and we determined the $K_{m,app}$ for C16:0-CoA to be 21.3 \pm 4.1 μM (see Extended Data Fig. 5c). Based on these data we have named CCNA 01212 bacterial Ceramide Synthase (bCerS). Since eukaryotic CerS enzymes have specific acyl-chain specificities 20 , we assessed the substrate preference of C. crescentus bCerS. Recombinant bCerS was incubated with 3-KDS and an equimolar mixture of acyl-CoA substrates ranging from C8-C24, and the relative amount of the respective products was monitored by LC/ESI-MS. C. crescentus had the highest in vitro activity with C14 and showed very little activity with acyl-CoA thioesters of 18 carbons or longer (see Extended Data Fig. 5d). In vivo, the C16 ceramide product is most abundant rather than C14 (see Extended Data Fig. 1e); this may reflect the fact that C16 accounts for 30% of the fatty acid content of the cell, whereas C14 is only 2%²¹. Our experiments demonstrating bCerS activity with acyl-CoA as a substrate are consistent with ceramide synthase activity; however, given that the acyl-CoA is readily hydrolyzed by bCerS to a free fatty acid, we cannot rule out the possibility that bCerS ligates the fatty acid to 3-KDS via a reverse-ceramidase-like mechanism²².

124

125

126

127

128

129

130

131

132

133

134

135

136

137

138

139

140

141

142

143

144

145

A common ceramide modification found in fungi, plants, some animal tissues, and bacteria is the addition of a hydroxyl group to form phytoceramides (4) (Fig. 1a). In plants, sphingoid base hydroxylase 1/2 (Sbh1/2) adds a hydroxyl group to sphinganine to form phytosphingosine (3) prior to the addition of the second acyl chain²³. In mammals, DES2 has dual Δ^4 -desaturase and C-4 hydroxylase activities enabling the hydroxylation of ceramide (5) to phytoceramide²⁴. C. crescentus does not have a homologue of Sbh1/2; DES2 has some homology to the fatty acid desaturase CCNA 03535, though deletion of ccna 03535 did not abolish ceramide hydroxylation. We did not identify any putative hydroxylases in our transposon screen; however, we hypothesized that this modification may not have a strong effect on one or both of our selection phenotypes. To focus on genes that promoted PMX-resistance only, we searched the Fitness Browser database²⁵ and found that the disruption of *ccna* 00202, a DesAfamily fatty acid desaturase/hydroxylase, results in PMX resistance. Deletion of ccna 00202 led to a ceramide molecule with a mass reduction of 16 Da corresponding to the loss of a hydroxyl group (Fig. 2d). Complementation of *ccna* 00202 restored ceramide hydroxylation (Fig. 2d). Tandem MS/MS data are consistent with the hydroxylation occurring on C2 of the acyl chain (see Extended Data Fig. 4). For this reason, we have named CCNA 00202 Ceramide Hydroxylase (CerH). Examination of the mass spectra of the CerR deletion mutant showed that hydroxylation remains in the absence of reduction (Fig. 2a). Mechanistically, this suggests that CerH can use either DHC or oxCer as a substrate, or that acyl chain hydroxylation occurs upstream of oxCer reduction.

147

148

149

150

151

152

153

154

155

156

157

158

159

160

161

162

163

164

165

166

167

168

169

The ceramide in *C. crescentus* has a monounsaturated acyl chain (see Extended Data Fig. 1e). Acyl chain desaturation has also been reported in *Sphingomonas* species²⁶. Attempts to identify a desaturase were unsuccessful. *C. crescentus* encodes at least four DesA-family

desaturases (*ccna_00203*, *ccna_01515*, *ccna_01743*, and *ccna_03535*). Deletion of each of these genes individually or in combination had no effect on ceramides. While there could be other, yet unidentified, desaturases, we hypothesized that *C. crescentus* bCerS may have a preference for monounsaturated acyl-CoA substrates. *In vitro*, recombinant bCerS had a 3-fold greater preference for C16:1-CoA over C16:0-CoA as a substrate (see Extended Data Fig. 5e); the saturated and monounsaturated C16 fatty acids are present in equal amounts *in vivo*²¹. *C. crescentus* encodes two orthologues each of FabA/FabB which are involved in the synthesis of monounsaturated fatty acids²⁷. These four genes are all essential²⁸ which precluded direct tests of our hypothesis. Since many bacteria produce fully saturated ceramides^{2,5}, it appears that this modification is not a universal feature of bacterial ceramide synthesis.

The observations of oxCer in the Δ*cerR* strain (Fig. 2a) and the ability of bCerS to use 3-KDS as a substrate (Fig. 2c) suggested that the order of the synthetic pathway in bacteria is different than that in eukaryotes. Based on the MS data, we can propose the following model for bacterial ceramide synthesis (Fig. 2e). Spt condenses serine with an acyl-thioester (either acyl-ACP or acyl-CoA) to produce 3-KDS. bCerS uses 3-KDS and a second palmitoyl-CoA to generate oxCer which is subsequently reduced to ceramide by CerR. We considered the possibility that CerR may work upstream of bCerS, as in eukaryotes. In this case, an alternative model is that bCerS can use either 3-KDS or sphinganine as a substrate leading to oxCer or ceramide as the final product, respectively. *In vitro* assays using recombinant bCerS show that the enzyme can use either substrate (Fig. 2c and Extended Data Fig. 5f). To determine which pathway was more likely to occur *in vivo*, we used fluorescently-tagged proteins to infer the subcellular localization of the synthetic enzymes. Incubation of bacteria with chloroform-saturated Tris buffer results in the preferential permeabilization of the outer membrane and

leakage of soluble periplasmic proteins²⁹ (Fig. 2f). Using this approach with the three core ceramide synthesis genes showed that Spt and bCerS retained fluorescence while the CerR signal was entirely lost (Fig. 2f). Consistent with the purification of recombinant Spt and bCerS as soluble proteins, these imaging studies suggest that Spt and bCerS are cytoplasmic whereas CerR is a soluble periplasmic protein. Though we cannot rule out other mechanisms, the spatial separation of these proteins *in vivo* is consistent with our model in which bCerS acts upstream of CerR (Fig. 2e).

Bacterial ceramides can be modified in a variety of species-specific manners including fatty acid hydroxylation (Fig. 2d), acyl chain branching², and head group modification by phosphorylation² or glycosylation⁴. In *C. crescentus*, we previously identified two sphingolipid glycosyltransferases⁴ and here we report the discovery of a ceramide hydroxylase CerH (Fig. 2d).

Bioinformatic identification of ceramide producing species

The identification of Spt, bCerS, and CerR as the core bacterial ceramide synthetic enzymes in *C. crescentus* presented the opportunity to find orthologues in other species and perform a bioinformatic screen for additional potential ceramide producers. Sphingolipids have been isolated from the oral pathogen *Porphyromonas gingivalis*³. The *spt* gene (*pgn_1721*) has been identified³ and BLAST analysis of bCerS and CerR suggested that PGN_0374 and PGN_1886 are the respective orthologues despite having limited homology (PGN_0374: 25% identical, 43% similar; PGN_1886: 23% identical, 43% similar). Additionally, unlike in *C. crescentus*, the proposed *P. gingivalis* genes are not in the same genomic locus. To test their functionality, we complemented *C. crescentus* deletion strains with the corresponding *P*.

gingivalis genes. Complementation with spt $(pgn_1721)^{30}$ yielded both the expected C. crescentus ceramide (m/z 588.465 Da) as well as a ceramide with two additional methylene units (m/z 614.478 Da) (Fig. 3a). These data are consistent with previous studies showing that P. gingivalis has a substrate preference for 17, 18, and 19-carbon fatty-acyl-CoA substrates³¹.

Complementation of $\Delta bcerS$ with pgn_0374 restored ceramide synthesis (Fig. 3b); a variety of ceramide molecules were observed suggesting that, like Spt, the P. gingivalis bCerS has different substrate preferences than the C. crescentus orthologue. Lastly, P. gingivalis cerR (pgn_1886) was able to rescue ceramide reduction (Fig. 3c). Together, these results demonstrate that screening for organisms with this set of genes could yield a broader set of bacteria with the potential to synthesize ceramides.

A BLAST analysis of Spt, bCerS and CerR against the NCBI prokaryotic representative genomes database (5,700+ representative bacterial organisms; see Materials and Methods and Supplementary Data 1 for detailed search parameters and E-value cutoffs) identified 272 organisms, belonging to 17 taxonomic classes, containing orthologues of all three genes (Fig. 3d, Supplementary Data 1, and Extended Data Fig. 6). Analysis of the distance between these core genes showed that, in most clades, the genes were within 10 kb of one another (see Extended Data Fig. 7a). However, among the Bacteroides these genes were found scattered throughout the genome (see Extended Data Fig. 7a); this is consistent with the high degree of chromosomal plasticity and genomic rearrangements associated with these organisms³². Whereas all previously identified ceramide producers are Gram-negative organisms, our bioinformatic analysis suggested that several Gram-positive Actinobacteria may be competent for ceramide synthesis. Lipidomic analyses confirmed the presence of dihydroceramide in *Streptomyces aurantiacus*, providing the first evidence of ceramide lipids in Gram-positive bacteria (Fig. 3e). MS/MS

analysis of *S. aurantiacus* showed that, in contrast to *C. crescentus*, fatty acid desaturation occurred on the long-chain base (LCB) (see Extended Data Fig. 7b). Based on phylogenetic clustering of the individual ceramide synthesis genes (Extended Data Fig. 6), as well as the fact that the three genes are found in a putative operon, it is possible that the ceramide synthesis cassette may have been acquired in these Actinobacteria by horizontal gene transfer from Deltaproteobacteria.

In eukaryotes, organisms often have multiple CerS isoforms with distinct fatty acyl-CoA specificities. For example, the six human CerS isoforms enable the synthesis of ceramides with acyl chain lengths of 14-26 carbons²⁰. We performed a bioinformatic search to identify bacterial species with multiple bCerS isoforms and found 22 candidates among the Alphaproteobacteria, Bacteroidia, Balneolia, Chitinophagia, and Rhodothermia (see Supplementary Data 2). In most cases, the two bCerS homologues were far apart on the chromosome making it impossible to know whether the two proteins were truly bCerS isoforms or simply similar N-acetyltransferases. One exception was *Prevotella buccae*, where the two candidate *bcerS* genes were encoded immediately next to one another (HMPREF0649_00885 and HMPREF0649_00886; 57% identical and 74% similar). We complemented the *C. crescentus ΔbcerS* strain with each of the *P. buccae* isoforms and found that while both could rescue ceramide synthesis, each enzyme produced distinct lipid products (Fig. 3f). HMPREF0649_00885 preferred a fully saturated LCB substrate while HMPREF0649_00886 used a desaturated LCB (see Extended Data Fig. 7c-d).

Independent evolution of ceramide production in bacteria

While the Spt enzyme catalytic residues are conserved between eukaryotic and bacterial species (see Extended Data Fig. 8), neither CerR nor bCerS share obvious homology to KDSR or

CerS, respectively. The closest eukaryotic homologue to CerR is NADH dehydrogenase 1A subcomplex subunit 9 (NDUF9A), which is a component of Complex I in the mitochondrial oxidative phosphorylation pathway. Conversely, the bacterial relatives of KDSR are annotated as short-chain dehydrogenases³³. While both reductase families have conserved catalytic and NAD-binding sites³⁴ (see Extended Data Fig. 9), human KDSR and *C. crescentus* CerR are only 27% similar and 14% identical. Phylogenetic clustering of these proteins showed that CerR evolved its ceramide reductase activity convergently, arising from NDUF9A-related genes (Fig. 4a).

Similarly, bCerS is a member of the GNAT family of acyltransferases. Bacteria have a variety of GNAT proteins which are closely related to eukaryotic Gcn5 acyltransferases. Phylogenetic analysis demonstrated that bCerS is a subgroup of bacterial GNATs whereas the eukaryotic CerS is only distantly related to Gcn5 family proteins (Fig. 4b). Indeed, eukaryotic CerS has a highly conserved Lag1P domain^{35,36} which is not found in any of the bCerS proteins (see Extended Data Fig. 10). These phylogenetic analyses, coupled with the proposed reordering of the synthetic pathway (Fig. 1a and 2f-g), demonstrate that ceramide synthesis evolved independently in bacteria and eukaryotes.

Discussion

Since the discovery of sphingolipids in the late 19th century by Johann L.W. Thudichum, thousands of publications have demonstrated these lipids to be ubiquitous throughout Eukarya; to date, there are over 500 published headgroup variants and acyl chain modifications among this lipid group (LIPID MAPS,³⁷). The diversity of sphingolipids reflects the multifunctional roles of these molecules: the sphingoid backbone provides structural integrity to the cell membrane, the

headgroups are involved in lipid-mediated interactions, and some sphingolipid-derivatives function as intracellular second messengers⁷.

284

285

286

287

288

289

290

291

292

293

294

295

296

297

298

299

300

301

302

303

304

305

306

The list of bacterial sphingolipid-producing species is comparatively short but growing. Their presence in several taxa begs the question of 'how widespread could this lipid be?'. Our results identify the key enzymes required for bacterial ceramide synthesis. While the Spt enzyme is homologous between prokaryotes and eukaryotes, bCerS and CerR are unique to bacteria. We note a recent publication also identified these genes as being involved in ceramide synthesis in C. crescentus¹². The authors proposed, without direct evidence, that these proteins carry out the same functions as their eukaryotic counterparts (see Reference ¹², Figure 11). However, our biochemical analyses demonstrate that CerR and bCerS have unique enzymatic activities and the sequence of synthetic reactions in the bacterial pathway is likely different than that in eukaryotes (Fig. 1a and 2f). The previous findings regarding bacterial ceramide synthesis are actually consistent with our proposed pathway; their thin-layer chromatography (TLC) analysis of the CerR deletion yielded an unidentified band which is likely oxCer (see Reference ¹², Figure 9, Δ1164, top-most band). Additionally, ectopic expression of Spt and CerR in E. coli did not yield sphinganine, while expression of Spt and bCerS did lead to the production of the fast migrating sphingolipid species (see Reference ¹², Figure S4). As this molecule does not occur in eukaryotes, they lacked a TLC standard to confirm the identity of this band leading to a challenge in interpreting the data.

Though our data support a mechanism in which bCerS directly adds an acyl chain to 3-KDS, we note that the metabolic intermediate sphinganine has been detected in *B*.

thetaiotaomicron². We have tried several lipid extraction methods as well as stable-isotope labeling but have never detected sphinganine in *C. crescentus*. While it is possible that the

ceramide synthesis pathway operates differently in *Bacteroides*, given the conservation of this enzyme as well as the ability of the *P. gingivalis* enzyme to complement the deletion in *C. crescentus* that seems less likely. An alternative hypothesis is that *Bacteroides* has a ceramidase enzyme, which is lacking in *C. crescentus*, that hydrolyzes ceramide to sphinganine. Indeed, a bioinformatic search identified two linear amide CN-hydrolases (pfam PF02275; of which ceramidases are members) in *B. thetaiotaomicron*. One of these enzymes hydrolyzes bile acids, however, the function of the second homologue is unknown³⁸. *C. crescentus* does not have a homologue of these proteins. Additionally, *B. thetaiotaomicron* can assimilate and metabolize sphinganine from the host gut to produce ceramide lipids³⁹. Not surprisingly, the details of SL biosynthesis vary in different bacteria and a working hypothesis is that that their environmental niches provide an opportunity for the utilization of particular SL metabolic pathways. Further characterization of the structures and mechanisms of these enzymes will be necessary to elucidate their physiological functions.

Coupled with phylogenetic analysis, our data support a model in which bacterial ceramide synthesis evolved convergently and independently of the eukaryotic pathway. This type of evolution, where identical substrates and products are metabolized by distinct enzymes, is well characterized particularly in plants. For example, 1) gibberellins (tetracyclic diterpenoid carboxylic acids) are produced by unique enzymes in plants and fungi⁴⁰, 2) several independent enzymatic pathways are used to produce caffeine among plant species⁴¹, and 3) the UDP-glucosyltransferases and β -glucosidases used in the synthesis of benzoxazinoids evolved independently in different plant lineages⁴². One potential mechanism for the independent evolution of metabolic pathways is gene duplication and modification of substrate specificity. In the case of bacterial ceramide synthesis, the CerR protein in *C. crescentus* is related to the NDUF9A-domain protein CCNA 03718 (27% identical and 46% similar). In this study, we

found that *P. buccae* encodes two bCerS proteins (57% identical and 74% similar) with unique substrate preferences (Fig. 3f).

Phylogenetic analysis of the three ceramide synthetic genes has identified a wide range of Gram-negative, as well as several Gram-positive, species with the potential to produce ceramides. These organisms occupy a range of habitats including aquatic, soil, and within animal hosts. Among the small subset of previously identified ceramide-producing species, these lipids play roles in outer membrane integrity⁴³, defense against bacteriophage⁴, protection against extracellular stress¹², suppression of host inflammation², and their production can be developmentally regulated⁵. Furthermore, lipidomic analyses of these organisms has identified a wide range of ceramide species with varying acyl chain length and saturation, acyl chain hydroxylation, and head group glycosylation and phosphorylation; the consequences of these modifications are yet to be determined. By defining the microbial blueprint for ceramide synthesis, we now have a platform for dissecting the physiological functions of these lipids and for potentially engineering the production of novel sphingolipids.

Acknowledgments: The authors thank Carla Cugini (Rutgers University) for providing *P. gingivalis* genomic DNA for cloning. The authors also thank Anthony Geneva (Rutgers University-Camden) for helpful discussions. Funding was provided by National Science Foundation grants MCB-1553004 and MCB-2031948 (E.A.K.), National Institutes of Health grants GM069338 and R01AI148366 (Z.G.), and Biotechnology and Biological Sciences Research Council grants BB/M010996/1 and BB/T016841/1 (D.J.C.).

Author contributions: G.S. made the mutant and complementation strains for characterizing the synthetic pathway and performed the lipid extractions. P.T., B.A., and E.C.M. purified and characterized the recombinant proteins. J.D.C. cloned and analyzed the *P. buccae* complementation strains. M.E.B.H. and E.A.K. performed the phylogenetic and bioinformatic analyses. E.A.K. acquired the microscopy images. A.C., R.D., L.F., and H.N. performed the transposon screen to isolate ceramide deficient mutants. Z.G. performed the lipid mass spectrometry analyses. G.S., P.T., B.A., Z.G., D.J.C., and E.A.K. designed the experiments, interpreted the data, and wrote the manuscript.

Competing interests: Authors declare no competing interests.

Figure Legends

Figure 1. CCNA_01220 is a functional serine palmitoyltransferase (Spt). (a) The schematic depicts the eukaryotic ceramide synthesis pathway. In some organisms, phytoceramides (4) are produced by adding a hydroxyl group (OH) to the sphingoid base (3) (Sph) or to ceramide (5) (DES2). (b) Recombinant Spt was incubated with the indicated substrates for 1 hr and reaction products were analyzed by MALDI-MS. The final panel shows a theoretical mass spectrum for the expected product, 3-KDS. (c) Kinetic analyses of Spt determined the Km for L-serine (upper) and C16:0-CoA (lower) (n=3; data are presented as mean +/- SD).

Figure 2. A genetic screen identified ceramide synthesis enzymes. (a-d) Negative ion ESI/MS shows the [M + Cl]⁻ ions of the lipids emerging at 2 to 3 min. Ceramide species are labelled with

a red dot and the modified lipid moiety is designated with a red-dashed oval. Note that MS/MS analysis of ceramide from C. crescentus shows that the desaturation occurs on the acyl chain (see Extended Data Fig. 1e); however, we have not determined the precise position of the double bond. In this, and all subsequent figures, the structural cartoons only indicate which acyl chain is desaturated, but not the exact position of the double bond. Relative quantification of all the major lipid species for each mass spectrum is available in Supplementary Table 3. (a) Lipids were extracted from wild-type, $\Delta ccna$ 01222, and ccna 01222-complemented cells. (b) Lipids were extracted from Δccna 01212 and ccna 01212-complemented cells. (c) Recombinant CCNA 01212 was incubated with 40 µM 3-KDS and 50 µM C16:0-CoA for 1 hr and the reaction product was analyzed by normal phase LC/ESI-MS in negative ion mode. (d) Lipids were extracted from $\triangle ccna$ 00202 and ccna 00202-complemented cells. (e) Based on the MS data above, we proposed the following model for bacterial ceramide synthesis. The genes comprising this synthetic pathway are in close proximity in the genome (see Extended Data Fig. 2b). (f) Cells expressing the indicated fluorescently-tagged proteins were grown overnight in the presence of inducer. GspG-mCherry and TAT-mCherry are control inner-membrane and periplasmic proteins, respectively. Control and permeabilized cells were imaged by fluorescence microscopy to monitor the loss of fluorescence upon permeabilization. The results are the overlay of phase and fluorescent images. Scale bar = $5 \mu m$.

394

395

396

397

398

376

377

378

379

380

381

382

383

384

385

386

387

388

389

390

391

392

393

Figure 3. Bioinformatic analysis identifies a wide range of potential ceramide-producing bacteria. (a-c) Deletions of the spt (a), bcerS (b), and cerR (c) genes in C. crescentus were complemented with the indicated homologues from P. gingivalis. Lipids extracted from these strains were analyzed by normal phase LC/ESI-MS in negative ion mode. $[M + C1]^-$ ions of the

ceramide species emerging at 2 to 3 min are shown with ceramide species labelled with a red dot. (d) Bacterial species with homologues to all three ceramide synthesis enzymes are clustered by the overall homology of the 3 proteins (see Methods). Bootstrap percentage values are indicated by shaded circles at each node. Branches are colored by taxonomic class and Gram-positive Actinobacteria are labeled. (e) Negative ion ESI/MS shows the [M + Cl]⁻ ions of the ceramide species (emerging at 2 to 3 min) extracted from *S. aurantiacus*. Ceramide is labelled with a red dot. Determination of the ceramide structure by MS/MS is provided in Extended Data Fig. 7b. (f) Deletion of *bcerS* in *C. crescentus* was complemented by two *bcerS* orthologues from *P. buccae*. [M + Cl]⁻ ions of the ceramide species emerging at 2 to 3 min are shown with ceramide species labelled with a red dot. Determination of the ceramide structures by MS/MS is provided in Extended Data Figs. 7c-d.

Unrooted trees built using the maximum likelihood method show the distance between eukaryotic and bacterial ceramide synthesis genes as well as their closest homologues. Bootstrap percentage values are indicated by shaded circles at each node. (a) Bacterial CerR is most closely related to eukaryotic and bacterial proteins of the NDUF9A family, a subunit of mitochondrial Complex I. By contrast, Eukaryotic KDSR is homologous to bacterial short-chain dehydrogenases, unrelated to CerR. (b) Bacterial bCerS is part of a larger family of GNAT acyltransferases, which are, in turn closely related to eukaryotic Gcn5 proteins. By contrast,

eukaryotic CerS proteins are distant from the Gcn5-related proteins.

Figure 4. Phylogenetic analysis indicates convergent evolution of ceramide synthesis. (a-b)

Data availability:

422

- The raw data for Figure 1C and Extended Data Figures 1c-d, 5c-e, and 7a are provided as
- 424 Microsoft Excel files in the supplementary information (Source Data 1-4). The data for the
- bioinformatic analyses was obtained from the following publicly available NCBI resources:
- 426 NCBI Prokaryotic Representative Genomes:
- https://ftp.ncbi.nlm.nih.gov/genomes/GENOME_REPORTS/prok_representative_genomes.txt.
- Accession numbers for the proteins used for BLAST analyses are as follows. Bacterial Spt
- homologues: C. crescentus YP 002516593.1; P. gingivalis BAG34240; M. xanthus ABF87747;
- 430 B. stolpii BAF73753. Bacterial bCerS homologues: C. crescentus YP 002516585.1; P.
- 431 gingivalis BAG32893; M. xanthus ABF92629; B. stolpii WP 102243213. Bacterial CerR
- homologues: C. crescentus YP 002516595.1; P. gingivalis BAG34405; M. xanthus ABF87537;
- 433 B. stolpii WP_102243212. Eukaryotic CerS homologues: Human P27544.1; A. thaliana
- NP 001184985; S. cerevisiae AAA21579.1. Eukaryotic Spt homologues: Human NP 006406.1;
- 435 A. thaliana NP 190447.1; S. cerevisiae CAA56805.1. Eukaryotic KDSR homologues: Human
- NP 002026.1; A. thaliana NP 187257; S. cerevisiae P38342. Eukaryotic Gcn5 homologues:
- 437 Human AAC39769.1 and *S. cerevisiae* NP_011768.1.

References

440

- Harrison, P. J., Dunn, T. M. & Campopiano, D. J. Sphingolipid biosynthesis in man and
- 442 microbes. *Nat Prod Rep* **35**, 921-954 (2018).
- Brown, E. M. et al. Bacteroides-derived sphingolipids are critical for maintaining
- intestinal homeostasis and symbiosis. *Cell Host Microbe* **25**, 668-680 e667 (2019).
- Moye, Z. D., Valiuskyte, K., Dewhirst, F. E., Nichols, F. C. & Davey, M. E. Synthesis of
- sphingolipids impacts survival of Porphyromonas gingivalis and the presentation of
- surface polysaccharides. *Front Microbiol* **7**, 1919 (2016).
- 448 4 Stankeviciute, G., Guan, Z., Goldfine, H. & Klein, E. A. Caulobacter crescentus adapts
- to phosphate starvation by synthesizing anionic glycoglycerolipids and a novel
- glycosphingolipid. *mBio* **10**, e00107-00119 (2019).
- 451 5 Ahrendt, T., Wolff, H. & Bode, H. B. Neutral and phospholipids of the *Myxococcus*
- 452 xanthus lipodome during fruiting body formation and germination. Appl Environ
- 453 *Microbiol* **81**, 6538-6547 (2015).
- Kaneshiro, E. S., Hunt, S. M. & Watanabe, Y. Bacteriovorax stolpii proliferation and
- predation without sphingophosphonolipids. *Biochem Biophys Res Commun* **367**, 21-25
- 456 (2008).
- Hannun, Y. A. & Obeid, L. M. Sphingolipids and their metabolism in physiology and
- 458 disease. *Nat Rev Mol Cell Biol* **19**, 175-191 (2018).
- 459 8 Merrill, A. H., Jr. Sphingolipid and glycosphingolipid metabolic pathways in the era of
- sphingolipidomics. *Chem Rev* **111**, 6387-6422 (2011).

- 461 9 Ikushiro, H., Hayashi, H. & Kagamiyama, H. A water-soluble homodimeric serine
- palmitoyltransferase from Sphingomonas paucimobilis EY2395T strain. Purification,
- characterization, cloning, and overproduction. *J Biol Chem* **276**, 18249-18256 (2001).
- 464 10 Yard, B. A. *et al.* The structure of serine palmitoyltransferase; gateway to sphingolipid
- 465 biosynthesis. *J Mol Biol* **370**, 870-886 (2007).
- 466 11 Geiger, O., Gonzalez-Silva, N., Lopez-Lara, I. M. & Sohlenkamp, C. Amino acid-
- 467 containing membrane lipids in bacteria. *Prog Lipid Res* **49**, 46-60 (2010).
- Olea-Ozuna, R. J. et al. Five structural genes required for ceramide synthesis in
- 469 *Caulobacter* and for bacterial survival. *Environ Microbiol* (2020).
- Wadsworth, J. M. *et al.* The chemical basis of serine palmitoyltransferase inhibition by
- 471 myriocin. J Am Chem Soc 135, 14276-14285 (2013).
- Harrison, P. J. et al. Use of isotopically labeled substrates reveals kinetic differences
- between human and bacterial serine palmitoyltransferase. *J Lipid Res* **60**, 953-962 (2019).
- Li, S., Xie, T., Liu, P., Wang, L. & Gong, X. Structural insights into the assembly and
- substrate selectivity of human SPT-ORMDL3 complex. *Nat Struct Mol Biol* **28**, 249-257
- 476 (2021).
- Raman, M. C. *et al.* The external aldimine form of serine palmitoyltransferase: structural,
- kinetic, and spectroscopic analysis of the wild-type enzyme and HSAN1 mutant mimics.
- 479 J Biol Chem **284**, 17328-17339 (2009).
- Raman, M. C., Johnson, K. A., Clarke, D. J., Naismith, J. H. & Campopiano, D. J. The
- serine palmitoyltransferase from Sphingomonas wittichii RW1: An interesting link to an
- unusual acyl carrier protein. *Biopolymers* **93**, 811-822 (2010).

study SPT activity in yeast Saccharomyces cerevisiae. J Lipid Res 59, 162-170 (2018). 484 19 Zheng, W. et al. Ceramides and other bioactive sphingolipid backbones in health and 485 disease: lipidomic analysis, metabolism and roles in membrane structure, dynamics, 486 signaling and autophagy. Biochim Biophys Acta 1758, 1864-1884 (2006). 487 20 Tidhar, R. et al. Eleven residues determine the acyl chain specificity of ceramide 488 synthases. J Biol Chem 293, 9912-9921 (2018). 489 21 Chow, T. C. & Schmidt, J. M. Fatty acid composition of Caulobacter crescentus. 490 491 Microbiology 83, 369-373 (1974). Okino, N. et al. The reverse activity of human acid ceramidase. J Biol Chem 278, 29948-22 492 29953 (2003). 493 23 Chen, M., Markham, J. E., Dietrich, C. R., Jaworski, J. G. & Cahoon, E. B. Sphingolipid 494 long-chain base hydroxylation is important for growth and regulation of sphingolipid 495 content and composition in Arabidopsis. *Plant Cell* **20**, 1862-1878 (2008). 496 24 Omae, F. et al. DES2 protein is responsible for phytoceramide biosynthesis in the mouse 497 small intestine. *Biochem J* **379**, 687-695 (2004). 498 25 Price, M. N. et al. Mutant phenotypes for thousands of bacterial genes of unknown 499 function. Nature 557, 503-509 (2018). 500 26 Kawahara, K., Moll, H., Knirel, Y. A., Seydel, U. & Zähringer, U. Structural analysis of 501 502 two glycosphingolipids from the lipopolysaccharide-lacking bacterium Sphingomonas

Ren, J. et al. Quantification of 3-ketodihydrosphingosine using HPLC-ESI-MS/MS to

483

503

18

capsulata. European Journal of Biochemistry 267, 1837-1846 (2000).

504 27 Feng, Y. & Cronan, J. E. Escherichia coli unsaturated fatty acid synthesis: complex transcription of the fabA gene and in vivo identification of the essential reaction catalyzed 505 by FabB. J Biol Chem 284, 29526-29535 (2009). 506 28 Christen, B. et al. The essential genome of a bacterium. Mol Syst Biol 7, 1-7 (2011). 507 29 Stankeviciute, G. et al. Differential modes of crosslinking establish spatially distinct 508 regions of peptidoglycan in Caulobacter crescentus. Mol Microbiol 111, 995-1008 509 (2019).510 30 Rocha, F. G. et al. Porphyromonas gingivalis sphingolipid synthesis limits the host 511 512 inflammatory response. J Dent Res 99, 568-576 (2020). 31 Mun, J. et al. Structural confirmation of the dihydrosphinganine and fatty acid 513 constituents of the dental pathogen Porphyromonas gingivalis. Org Biomol Chem 5, 514 3826-3833 (2007). 515 32 Nguyen, M. & Vedantam, G. Mobile genetic elements in the genus Bacteroides, and their 516 mechanism(s) of dissemination. *Mob Genet Elements* 1, 187-196 (2011). 517 33 Kavanagh, K. L., Jornvall, H., Persson, B. & Oppermann, U. Medium- and short-chain 518 dehydrogenase/reductase gene and protein families: the SDR superfamily: functional and 519 structural diversity within a family of metabolic and regulatory enzymes. Cell Mol Life 520 Sci 65, 3895-3906 (2008). 521 Boyden, L. M. et al. Mutations in KDSR cause Recessive Progressive Symmetric 522 34 523 Erythrokeratoderma. *Am J Hum Genet* **100**, 978-984 (2017). Kageyama-Yahara, N. & Riezman, H. Transmembrane topology of ceramide synthase in 35 524 yeast. Biochem J 398, 585-593 (2006). 525

- 526 36 Spassieva, S. *et al.* Necessary role for the Lag1p motif in (dihydro)ceramide synthase
- activity. J Biol Chem **281**, 33931-33938 (2006).
- Liebisch, G. et al. Update on LIPID MAPS classification, nomenclature and shorthand
- notation for MS-derived lipid structures. *J Lipid Res* (2020).
- Yao, L. et al. A selective gut bacterial bile salt hydrolase alters host metabolism. Elife 7
- 531 (2018).
- Lee, M. T., Le, H. H. & Johnson, E. L. Dietary sphinganine is selectively assimilated by
- members of the mammalian gut microbiome. *J Lipid Res* **62**, 100034 (2021).
- Tudzynski, B. Gibberellin biosynthesis in fungi: genes, enzymes, evolution, and impact
- on biotechnology. *Appl Microbiol Biotechnol* **66**, 597-611 (2005).
- Huang, R., O'Donnell, A. J., Barboline, J. J. & Barkman, T. J. Convergent evolution of
- caffeine in plants by co-option of exapted ancestral enzymes. *Proc Natl Acad Sci U S A*
- **113**, 10613-10618 (2016).
- 539 42 Dick, R. et al. Comparative analysis of benzoxazinoid biosynthesis in monocots and
- dicots: independent recruitment of stabilization and activation functions. *Plant Cell* **24**,
- 541 915-928 (2012).

548

- Kawasaki, S. et al. The cell envelope structure of the lipopolysaccharide-lacking gram-
- negative bacterium Sphingomonas paucimobilis. *J Bacteriol* **176**, 284-290 (1994).
- Madeira, F. *et al.* The EMBL-EBI search and sequence analysis tools APIs in 2019.
- 545 Nucleic Acids Res (2019).
- Lowther, J. et al. Role of a conserved arginine residue during catalysis in serine

25

palmitoyltransferase. *FEBS Lett* **585**, 1729-1734 (2011).

Materials and Methods

Bacterial strains, plasmids, and growth conditions

The strains, plasmids, and primers used in this study are described in Supplementary Tables 4, 5, and 6, respectively. Strain construction details are available in a Supplementary Note. *C. crescentus* wild-type strain NA1000 and its derivatives were grown at 30 °C in peptone-yeast-extract (PYE) medium for routine culturing. To control serine concentration for the serine auxotrophic strain, *C. crescentus* was grown in Hutner-Imidazole-Glucose-Glutamate (HIGG) media⁴⁶ with variable amounts of serine (0-10 mM). *E. coli* strains were grown at 37 °C in LB medium. When necessary, antibiotics were added at the following concentrations: kanamycin 30 μg/ml in broth and 50 μg/ml in agar (abbreviated 30:50) for *E. coli* and 5:25 for *C. crescentus*; tetracycline 12:12 *E. coli* and 1:2 *C. crescentus*; spectinomycin 50:50 *E. coli* and 25:100 *C. crescentus*; and ampicillin 50:100 *E. coli*. Gene expression was induced in *C. crescentus* with either 0.3% (w/v) xylose or 0.5 mM vanillate. *Streptomyces aurantiacus* was grown in International Streptomyces Project Synthetic Salts-Starch Medium (ISP4) at 30 °C.

Genetic screen for ceramide synthesis enzymes

A conjugation-competent and diaminopimelic acid (DAP) auxotrophic strain of *E. coli* (MFDpir, ⁴⁷) carrying the kanamycin-encoding mini-Tn5 plasmid pBAM1 (Addgene #60487, ⁴⁸) was grown overnight in LB media containing 0.3 mM DAP. Wild-type *C. crescentus* was grown overnight in PYE. In a microcentrifuge tube, 1 ml of *C. crescentus* was mixed with 100 μl of *E. coli*, the cells were washed once in PYE, and the final cell pellet was resuspended in 20 μl PYE. The concentrated cell sample was dropped onto a PYE agar plate containing 0.3 mM DAP and

incubated at 30 °C for 6 hr. After incubation, the cells were scraped into 1 ml of PYE, vortexed, and spread onto PYE agar plates containing 25 µg/ml kanamycin and 200 µg/ml polymyxin B. In the absence of DAP, the donor E. coli strain could not grow, the kanamycin selected for transposon insertions, and the polymyxin B selected for potentially ceramide-deficient cells. Colonies were picked into duplicate 96-well plates containing 200 µl PYE per well +/- 2 µl bacteriophage ϕ Cr30. Each plate had one well of wild-type control and one well with no cells, as a control for contamination. Approximately 20 sets of duplicate plates were inoculated. Plates were incubated overnight at 30 °C and growth was measured in a BMG Labtech CLARIOstar plate reader by absorbance at 660 nm. The 94 phage-containing wells that had the lowest OD_{660} were considered potential hits. The corresponding wells from the non-infected plates were consolidated into new 96-well plates and treated +/- phage as above. Growth curves were acquired for 27 hr on a BMG Labtech CLARIOstar plate reader incubating at 30 °C with shaking. The ratio of the final to the maximal OD₆₆₀ for each well was calculated and normalized to the wild-type control. Wells with a ratio less than that of the wild-type control were kept for further characterization. To determine the site of transposon insertion we used arbitrarily-primed PCR with primer pairs EKS153/S159 and EKS154/S160 as previously described⁴⁸.

588

589

590

591

592

593

594

572

573

574

575

576

577

578

579

580

581

582

583

584

585

586

587

Cloning and purification of C. crescentus Spt

The *ccna_01220* gene was amplified with primers EK1107/1108. A C-terminal 6-histidine tag expression vector (pET-28a, EMD Biosciences) was amplified with primers EK1131/1106 and the insert was ligated using HiFi Assembly (New England Biolabs). The resulting plasmid was transformed into *E. coli* BL21 (DE3) cells. One colony was grown overnight in Terrific Broth (TB)/kanamycin at 37 °C with shaking. The inoculant was diluted into TB/kanamycin to OD₆₀₀

of 0.1. When the OD₆₀₀ reached 0.8, protein expression was induced with 0.5 mM isopropyl- β -D-1-thiogalactopyranoside (IPTG), and cultures were grown at 16 °C overnight. Cells were harvested by centrifugation at 5,000 x g for 7 min. The cell pellets were resuspended in 20 mM potassium phosphate buffer, pH 7.5, 250 mM NaCl, 30 mM imidazole and 25 μ M pyridoxal phosphate (PLP). The cells were sonicated on ice (Soniprep 150, 10 cycles of 30 seconds on/30 seconds off), cell lysates were cleared by centrifugation at 24,000 x g for 40 min, and supernatants were filtered through a 0.45 μ m filter. The recombinant Spt was purified using an Äkta FPLC system (Cytiva) and a HisTrap HP 1 ml Ni²⁺ column (Cytiva) with an imidazole gradient from 30 mM to 500 mM, followed by size exclusion chromatography (SEC) on a HiLoad 16/600 Superdex 200 preparatory grade column (Cytiva) with a buffer containing 20 mM potassium phosphate, pH 7.5, 250 mM NaCl, 10% (v/v) glycerol and 25 μ M PLP. The purification was monitored by SDS-PAGE and Coomassie blue staining.

Cloning and purification of C. crescentus bCerS

The *ccna_01212* gene was amplified with primers EK1199/1269 and cloned into the Ndel/HindIII site of plasmid pET-28a to generate an N-terminal 6-histidine tag. The construct was transformed into *E. coli* BL21 (DE3) competent cells. One colony was grown overnight in LB broth/kanamycin at 37 °C with shaking. The inoculant was diluted into LB/kanamycin to OD₆₀₀ of 0.1. When the OD₆₀₀ reached 0.8, protein expression was induced with 1 mM IPTG, and cultures were grown at 16 °C overnight. Cells were harvested by centrifugation at 5,000 x *g* for 7 min. The cell pellets were resuspended in 50 mM Tris-HCl, pH 8.0, 250 mM NaCl, and 30 mM imidazole. The cells were sonicated on ice (Soniprep 150, 10 cycles of 30 seconds on/30 seconds off), cell lysates were cleared by centrifugation at 24,000 x *g* for 40 min, and

supernatants were filtered through a 0.45 µm filter. The recombinant bCerS was purified using an Äkta FPLC system (Cytiva) and a HisTrap HP 1 ml Ni²⁺ column (Cytiva) with an imidazole gradient from 10 mM to 500 mM, followed by size exclusion chromatography (SEC) on a HiLoad 16/600 Superdex 200 preparatory grade column (Cytiva) with a buffer containing 50 mM Tris-HCl, pH 8.0, 250 mM NaCl, and 10% (v/v) glycerol. The purification was monitored by SDS-PAGE and Coomassie blue staining.

Mass Spectrometry of recombinant proteins

Purified Spt and bCerS were analyzed in positive ion mode using a liquid chromatography system connected to a Waters Synapt G2 QTOF with an electrospray ionization (ESI) source. 10 μL of 10 μM protein was injected into a Phenomenex C4 3.6 μm column. The conditions for the qTOF were source temperature 120 °C, backing pressure 2 mbar, and sampling cone voltage 54V. The protein was eluted with a 12-minute gradient, starting at 5% acetonitrile with 0.1% formic acid to 95% acetonitrile. The resulting spectra were analyzed using MassLynx V4.1 software (Waters Corporation)

Determination of kinetic constants for C. crescentus Spt

Spt kinetic parameters were determined using a 5,5'-dithiobis-(2-nitrobenzoic acid) (DTNB) assay as previously described ¹⁶. The enzyme kinetic assay was carried out in a 96 well microtiter plate containing 0.4 mM DTNB, 1 μ M Spt enzyme, 20 mM L-serine, 1-1000 μ M C16:0/1-CoA for K_m-C16:0/1-CoA determination or 0.4 mM DTNB, 1 μ M Spt enzyme, 0.1-100 mM L-serine, 250 μ M C16:0/1-CoA for K_m-L-Ser determination in a buffer containing 100 mM HEPES, 250 mM NaCl, pH 7.0. The experiments were monitored in a BioTek Synergy HT plate reader at 412

nm in 1 min intervals for 60 minutes at 30 °C. The enzyme kinetic constants were calculated by fitting the Michaelis-Menten equation to a plot of reaction rate versus concentration using Origin 2019 (OriginLab).

Assessing sphingolipid products using MALDI-TOF-MS

Spt reaction products were desalted using OMIX C4 pipette tips (Agilent) and eluted in 100% acetonitrile (ACN) containing 0.2% formic acid. 1 μL of first matrix seed (20 mg/ml alphacyano-4-hydroxycinnamic acid (CHCA) in methanol/acetone (2:3, v/v) was spotted onto a MTP 384 ground steel plate (Bruker) and left to air dry. The samples were mixed with the second matrix (20 mg/ml CHCA in 50% ACN within 0.25% trifluoroacetic acid (TFA)) in a 1:1 ratio, and 1 μL of the mixture was spotted on top of the CHCA-acetone layer and left to air-dry. The samples were analyzed in reflector mode using a calibrated Bruker UltrafleXtreme MALDI-TOF-mass spectrometer. The analysis was carried out in positive ion mode. The laser power was adjusted to provide optimum signal. Each sample was tested with 500 laser shots and each spectrum was a sum of over 5000 shots. Spectra were acquired over a range of *m/z* 200-1500. The data acquisition software used was Flex Control version 3.4. The data was analyzed using Data Analysis version 4.4 software.

Enzymatic activity assay for C. crescentus bCerS

The reactions were carried out with 2 μ M bCerS, 40 μ M 3-ketodihydrosphingosine (3-KDS) (dissolved in 0.1% v/v ethanol) and 50 μ M C16-CoA for at least 1 hour in a buffer containing 20 mM HEPES, 25 mM KCl, 2 mM MgCl₂, pH 7.5. The reaction products were extracted using the Bligh-Dyer method⁴⁷ and characterized by LC/MS as described below. To assay bCerS substrate

specificity, the reaction was carried out as above using equimolar amounts of C8-C24-CoA (total acyl-CoA concentration remained 50 μ M).

Determination of kinetic constants for C. crescentus bCerS

bCerS kinetic parameters were determined using a DTNB assay as previously described above for Spt. The enzyme kinetic assay was carried out in a 96 well microtiter plate containing 1 mM DTNB, 1.2 mg/ml bCerS enzyme, 0 or 40 μ M 3-KDS, and 1-500 μ M C16:0-CoA for K_m-C16:0-CoA determination in a buffer containing 100 mM HEPES, 150 mM NaCl, pH 7.5. The experiments were monitored in a BioTek Synergy HT plate reader at 412 nm in 30 second intervals for 60 minutes at 30 °C. The enzyme kinetic constants were calculated by fitting the Michaelis-Menten equation to a plot of reaction rate versus concentration using Origin 2019 (OriginLab).

Lipid extraction

C. crescentus strains were grown overnight (5 ml) and lipids were extracted by the method of Bligh and Dyer⁴⁹. Cells were harvested in glass tubes at $10,000 \times g$ for 30 min and the supernatant was removed. The cells were resuspended in 1 ml of water, 3.75 volumes of 1:2 (v/v) chloroform: methanol was added, and the samples were mixed by vortexing. Chloroform (1.25 volumes) and water (1.25 volumes) were added sequentially with vortexing to create a two-phase system and the samples were centrifuged at $200 \times g$ for 5 minutes at room temperature. The bottom, organic phase was transferred to a clean tube with a Pasteur pipette and washed twice in "authentic" upper phase. Subsequently, the residual organic phase with the lipids was collected and dried under argon.

Lipid analysis by normal phase LC/ESI-MS/MS

Methods for lipid analysis by normal phase LC/ESI–MS/MS have been described spiriting. Briefly, normal phase LC was performed on an Agilent 1200 Quaternary LC system equipped with an Ascentis Silica HPLC column, 5 μ m, 25 cm × 2.1 mm (Sigma-Aldrich, St. Louis, MO) as described. The LC eluent (with a total flow rate of 300 μ l/min) was introduced into the ESI source of a high resolution TripleTOF5600 mass spectrometer (Applied Biosystems, Foster City, CA). Instrumental settings for negative ion ESI and MS/MS analysis of lipid species were as follows: ion spray voltage (IS) = -4500 V; curtain gas (CUR) = 20 psi; ion source gas 1 (GSI) = 20 psi; declustering potential (DP) = -55 V; and focusing potential (FP) = -150 V. The MS/MS analysis used nitrogen as the collision gas. Data analysis was performed using Analyst TF1.5 software (Applied Biosystems, Foster City, CA). A list of the identified lipid species can be found in Supplementary Table 2. A representative total ion chromatogram (TIC) and its corresponding extracted ion chromatogram (EIC) is available in Extended Data Figs. 3c-d. The peak areas of the EICs of major lipid species are compiled in Supplementary Table 3.

Cell permeabilization and labeling

Chloroform-saturated Tris buffer was prepared by mixing 50 mM Tris, pH 7.4 with chloroform (70:30) and shaking the mixture at room temperature for 30 min. Cells to be permeabilized were collected via centrifugation (2 min at 6,000 x g, 4 °C) and resuspended in an equal volume of the aqueous phase of the chloroform-saturated Tris buffer. Resuspended cells were rocked for 45 min at room temperature and then washed twice in 50 mM Tris, pH 7.4 (via centrifugation for 10

min at 5,000 x g) to remove residual chloroform. Control cells were treated as above, but incubated in 50 mM Tris, pH 7.4 without chloroform.

Fluorescence microscopy

Cells harboring fluorescent fusions were induced overnight with 0.3% xylose and permeabilized as described above. The permeabilizes cells were spotted onto 1% agarose pads. Fluorescence microscopy was performed on a Nikon Ti-E inverted microscope equipped with a Prior Lumen 220PRO illumination system, CFI Plan Apochromat 100X oil immersion objective (NA 1.45, WD 0.13 mm), Zyla sCMOS 5.5-megapixel camera (Andor), and NIS Elements v, 4.20.01 for image acquisition.

Phylogenetic analysis of bacterial ceramide synthesis genes

Following our identification of Spt, bCerS, and CerR as key enzymes in ceramide synthesis in *C. crescentus*, we used BLASTP to find the closest protein homologues in the known ceramide producers *P. gingivalis*, *M. xanthus*, and *B. stolpii* (see Supplementary Data 1). Using each of these proteins as a query, we used TBLASTN to find related proteins in the NCBI prokaryotic representative genomes database (5,700+ representative bacterial organisms). E-value cutoffs were determined by performing a traditional BLASTP with each protein and getting the approximate E-value cutoff for the top 250 hits (see Supplementary Data 1). TBLASTN settings were chosen to only take the top hit for each organism, and we collected the organism name, taxonomic ID, sequence start and end position, strand orientation, and protein sequence.

Following the TBLASTN searches, the data were combined and filtered to remove duplicates. We identified organisms that contained hits for all three target genes. To facilitate comparison of

these organisms, we made *in silico* fusions by concatenating the Spt, CerR, and bCerS protein sequences. These fused sequences were aligned using MUSCLE aligner⁵¹. Phylogenetic trees were prepared using RAxML (Randomized Axelerated Maximum Likelihood version 8.2.12)⁵² with 100 bootstraps and a maximum-likelihood search. RAxML was run on the CIPRES Portal at the San Diego Supercomputer Center⁵³. Similar phylogenetic analyses were performed for the individual enzymes (see Extended Data Fig. 6). The taxonomic class for each organism was retrieved from the NCBI taxonomy database using the R package taxize⁵⁴. Phylogenetic trees were visualized in R using the packages ggtree⁵⁵, ape⁵⁶, treeio⁵⁷, and ggplot2⁵⁸.

Phylogenetic analyses of ceramide synthesis genes

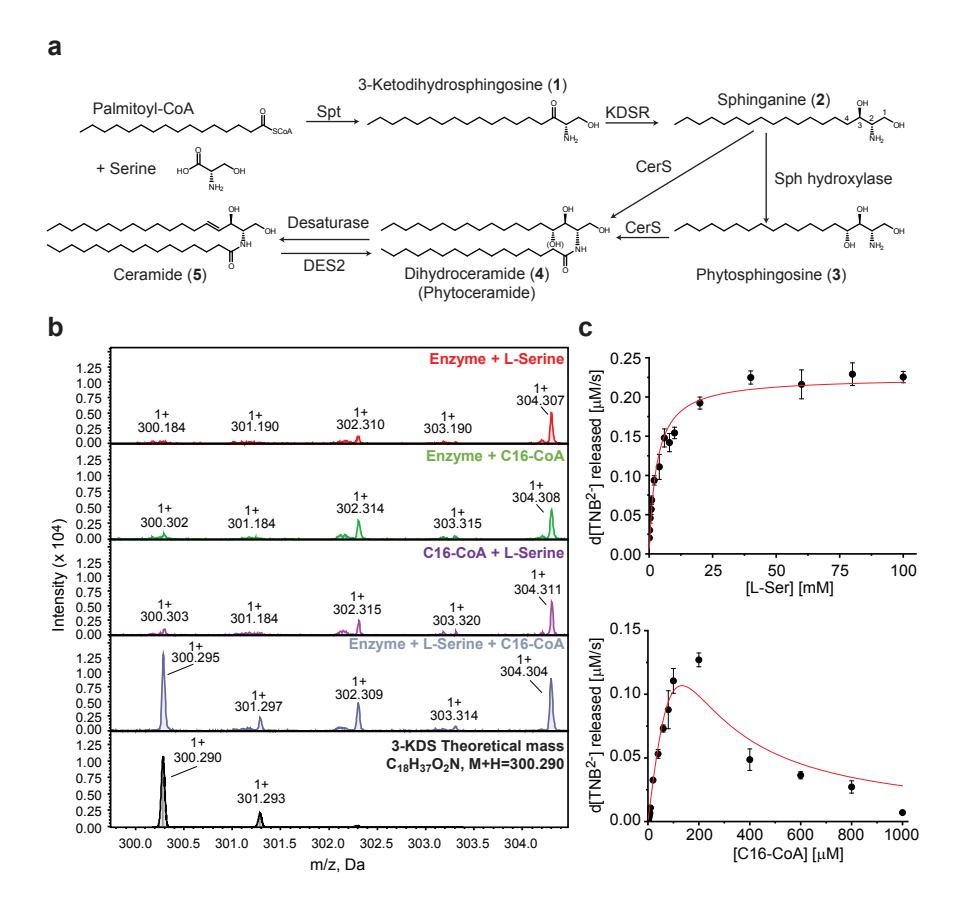
To get a representative set of sequences from across the eukaryotic domain, we used BLASTP on the NCBI server to find the top 500 eukaryotic hits for CerS from humans (CerS1, Accession P27544.1), *Arabidopsis thaliana* (Lag1P, Accession NP_001184985), and *Saccharomyces cerevisiae* (Lag1P, Accession AAA21579.1). The results were cleaned to remove duplicate hits; in order to compare roughly the same number of proteins in each group, 250 hits were chosen at random using the Linux "shuf" command. The same protocol was used for the following Spt and KDSR queries: human (Accessions NP_006406.1 and NP_002026.1), *A. thaliana* (Accessions NP_190447.1 and NP_187257), and *S. cerevisiae* (Accessions CAA56805.1 and P38342). The yeast CerS and KDSR proteins were then used to find the closest homologues in bacteria using BLASTP. Short-chain dehydrogenases similar to yeast KDSR were identified; by contrast, yeast CerS had a single partial match (45% query coverage, E-value=4.0) in *Orenia metallireducens*. *C. crescentus* CerR was used as a query to find the closest eukaryotic homologues, which identified NDUF9A proteins. A reverse-BLAST identified CCNA 03718 as the closest *C*.

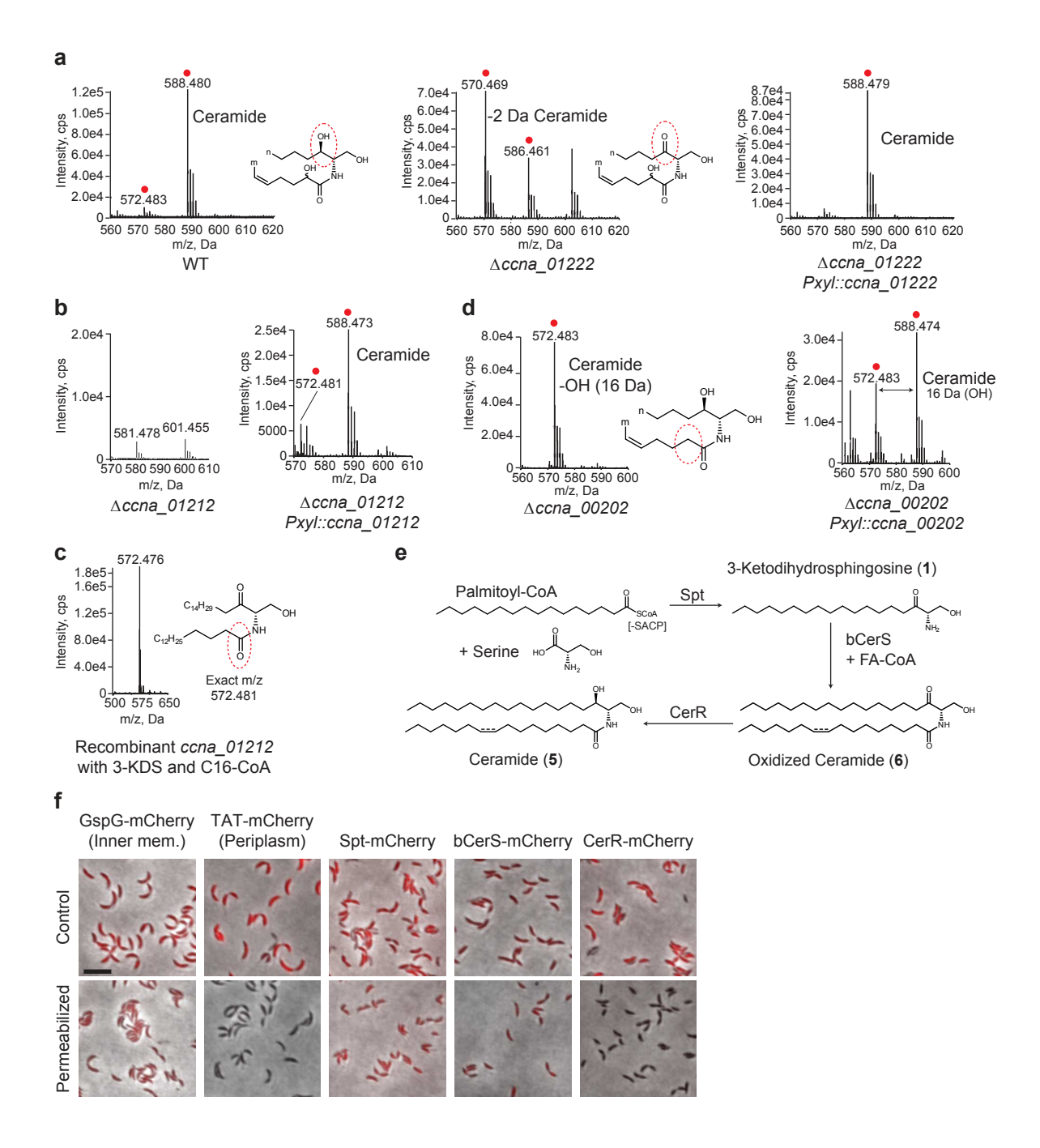
crescentus NDUF9A homologue, which was then used to identify other bacterial NDUF9A homologues. To trace the lineage of bCerS, we used the following protein queries to identify eukaryotic Gcn5 proteins: human (Accession AAC39769.1) and *S. cerevisiae* (Accession NP_011768.1). We identified bacterial GNAT proteins using *C. crescentus* bCerS as a BLASTP query to search the entire NCBI bacterial database. The eukaryotic Spt proteins were compared to the bacterial Spt proteins identified in Supplemental Data 1. Phylogenetic trees for the Spt, CerR/KDSR/NDUF9A, and CerS/Gcn5/GNAT/bCerS proteins were prepared with MUSCLE and RAxML and visualized with R as described above.

Methods references

- Poindexter, J. S. Selection for nonbuoyant morphological mutants of *Caulobacter* crescentus. *J Bacteriol* **135**, 1141-1145 (1978).
- Ferrieres, L. *et al.* Silent mischief: bacteriophage Mu insertions contaminate products of
 Escherichia coli random mutagenesis performed using suicidal transposon delivery
 plasmids mobilized by broad-host-range RP4 conjugative machinery. *J Bacteriol* **192**,
 6418-6427 (2010).
- Martinez-Garcia, E., Calles, B., Arevalo-Rodriguez, M. & de Lorenzo, V. pBAM1: an all-synthetic genetic tool for analysis and construction of complex bacterial phenotypes.
- *BMC Microbiol* **11**, 38 (2011).
- 774 49 Bligh, E. G. & Dyer, W. J. A rapid method of total lipid extraction and purification. *Can*775 *J Biochem Physiol* **37**, 911-917 (1959).

- Guan, Z., Katzianer, D., Zhu, J. & Goldfine, H. Clostridium difficile contains
- 777 plasmalogen species of phospholipids and glycolipids. *Biochim Biophys Acta* **1842**, 1353-
- 778 1359 (2014).
- Edgar, R. C. MUSCLE: a multiple sequence alignment method with reduced time and
- space complexity. *BMC Bioinformatics* **5**, 113 (2004).
- 52 Stamatakis, A. RAxML version 8: a tool for phylogenetic analysis and post-analysis of
- 782 large phylogenies. *Bioinformatics* **30**, 1312-1313 (2014).
- 783 53 Miller, M. A., Pfeiffer, W. & Schwartz, T. Creating the CIPRES Science Gateway for
- inference of large phylogenetic trees. 2010 Gateway Computing Environments Workshop
- 785 *(GCE)*, 1-8 (2010).
- Chamberlain, S. A. & Szocs, E. taxize: taxonomic search and retrieval in R. F1000Res 2,
- 787 191 (2013).
- 788 55 Yu, G. Using ggtree to visualize data on tree-like structures. *Curr Protoc Bioinformatics*
- 789 **69**, e96 (2020).
- Paradis, E. & Schliep, K. ape 5.0: an environment for modern phylogenetics and
- evolutionary analyses in R. *Bioinformatics* **35**, 526-528 (2019).
- Wang, L. G. et al. Treeio: An R Package for phylogenetic tree input and output with
- richly annotated and associated data. *Mol Biol Evol* **37**, 599-603 (2020).
- 794 58 Wickham, H. ggplot2: Elegant Graphics for Data Analysis. (Springer-Verlag New York,
- 795 2016).





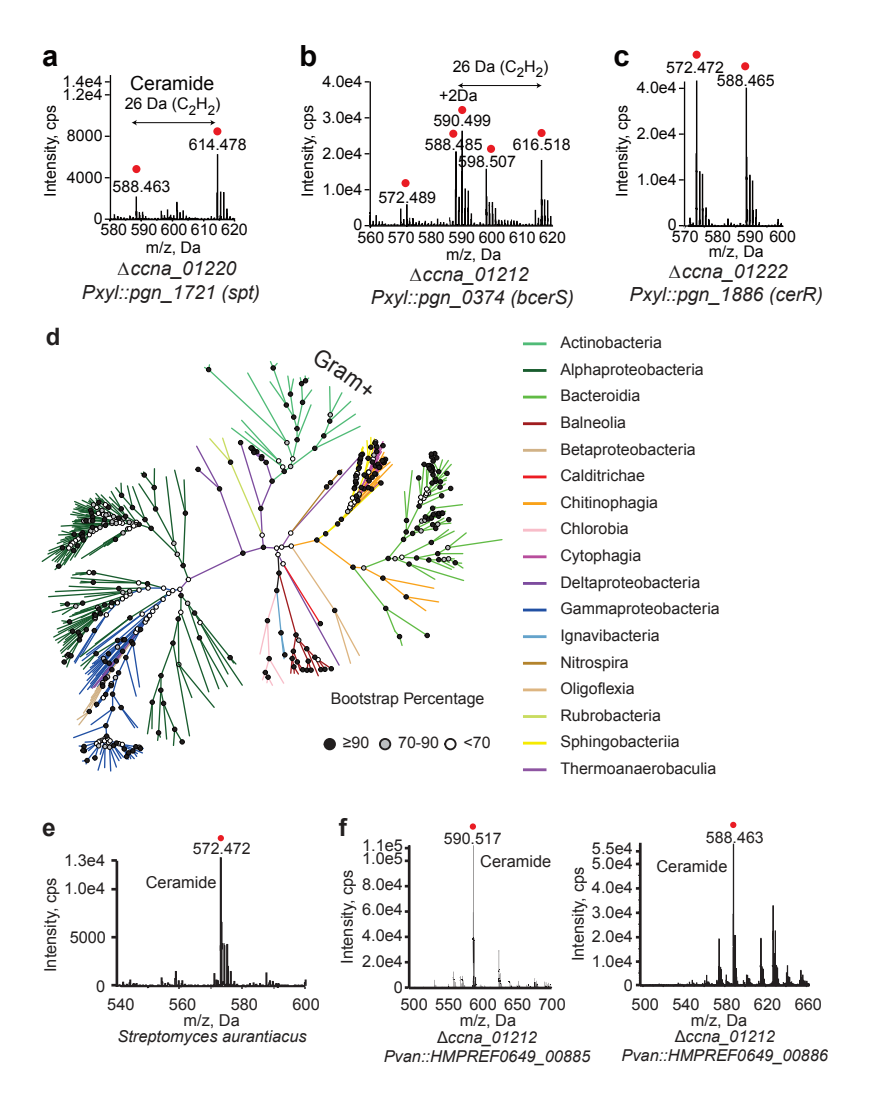
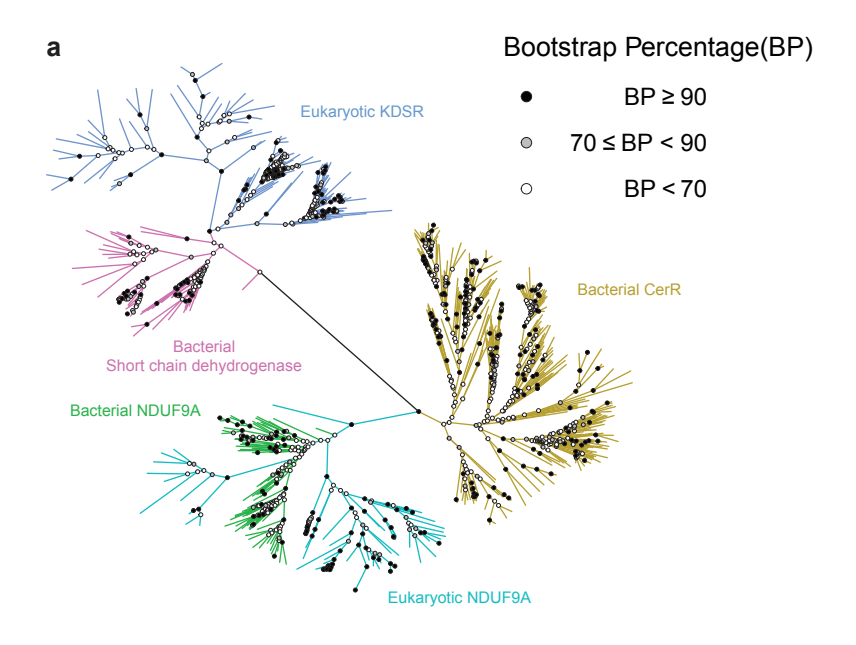
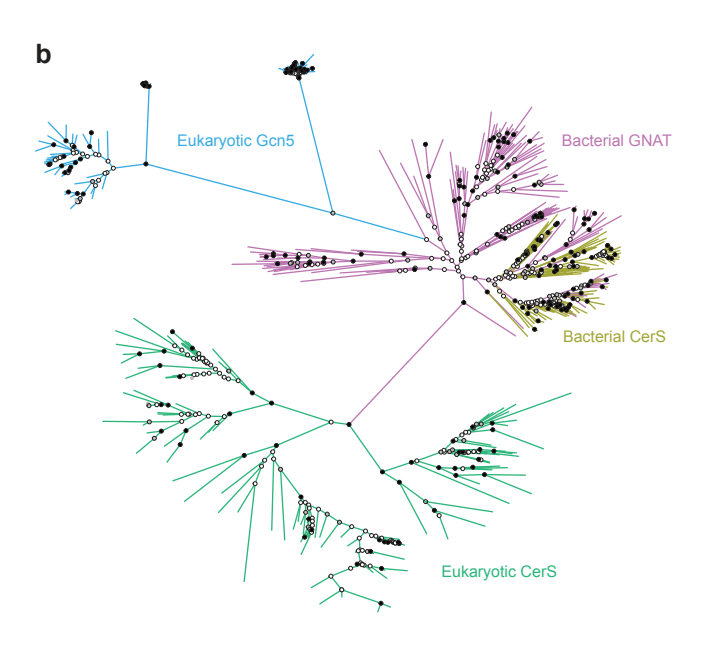
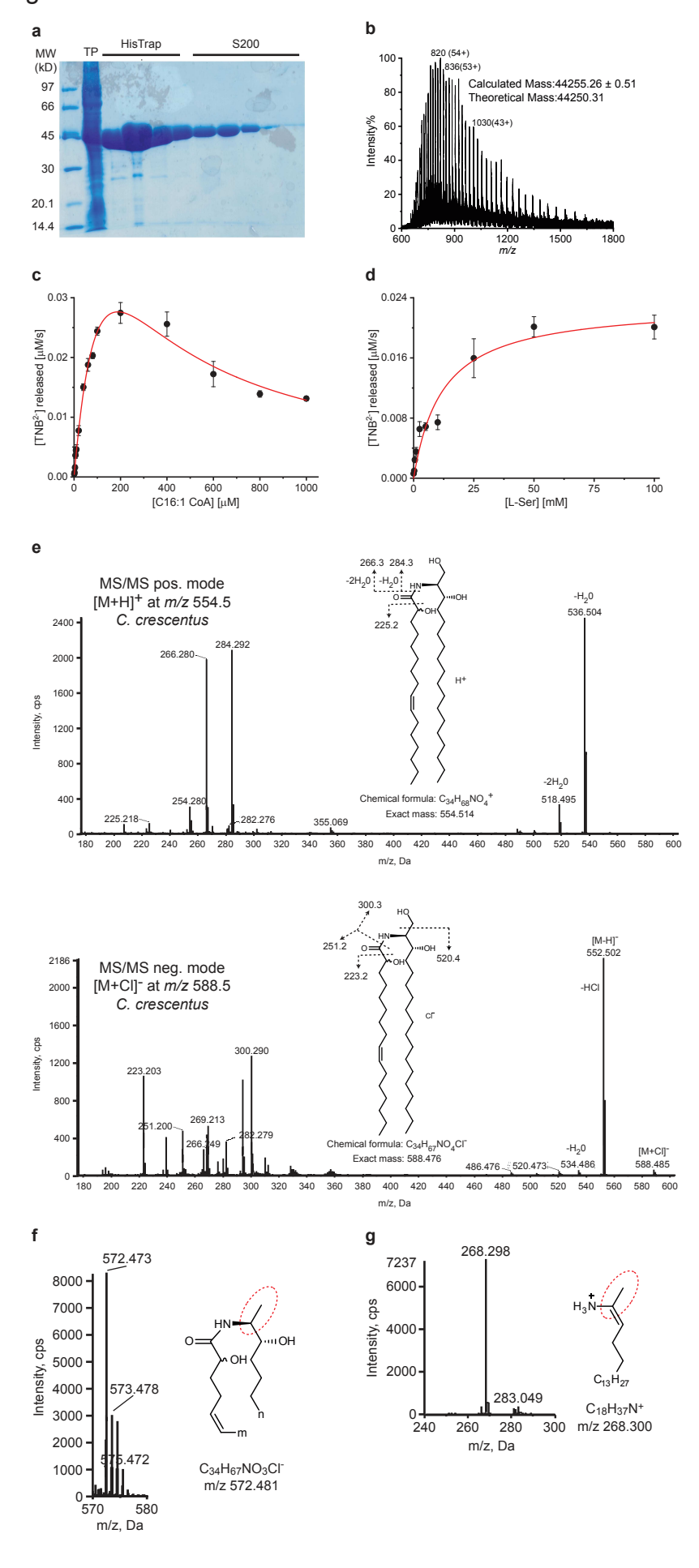


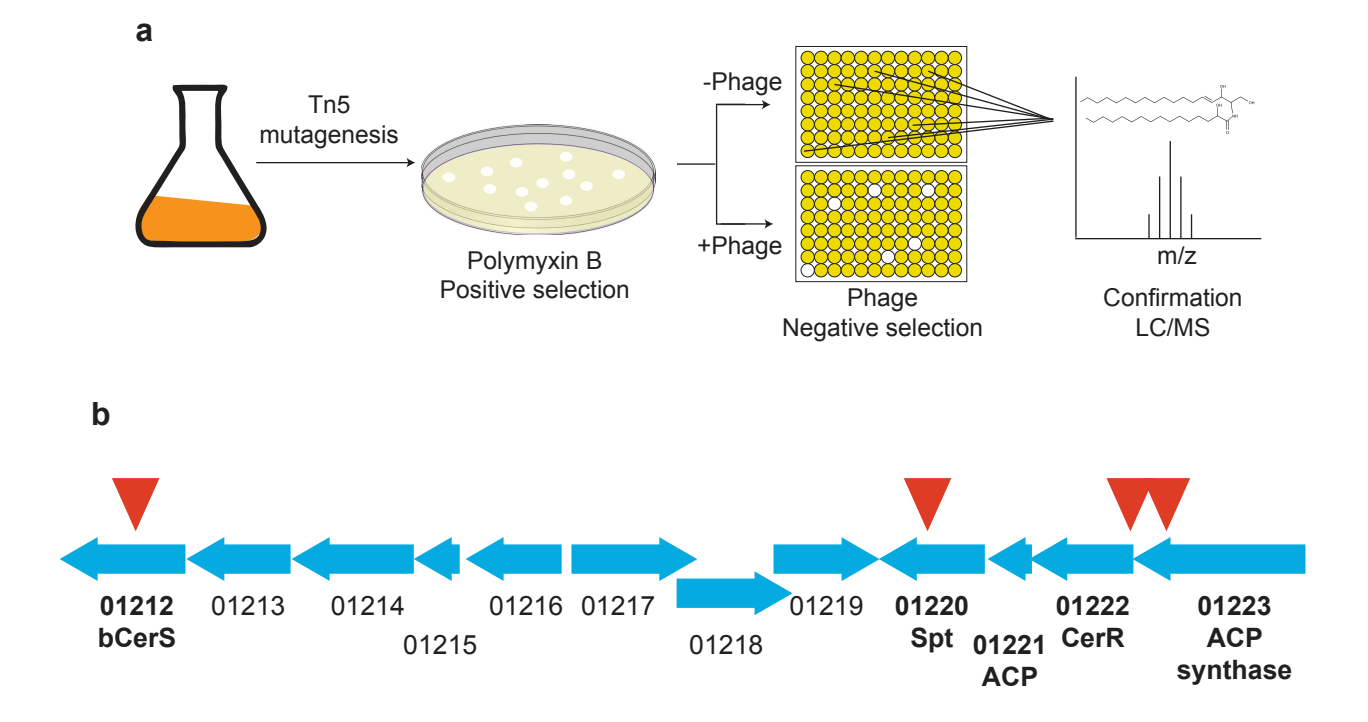
Figure 4

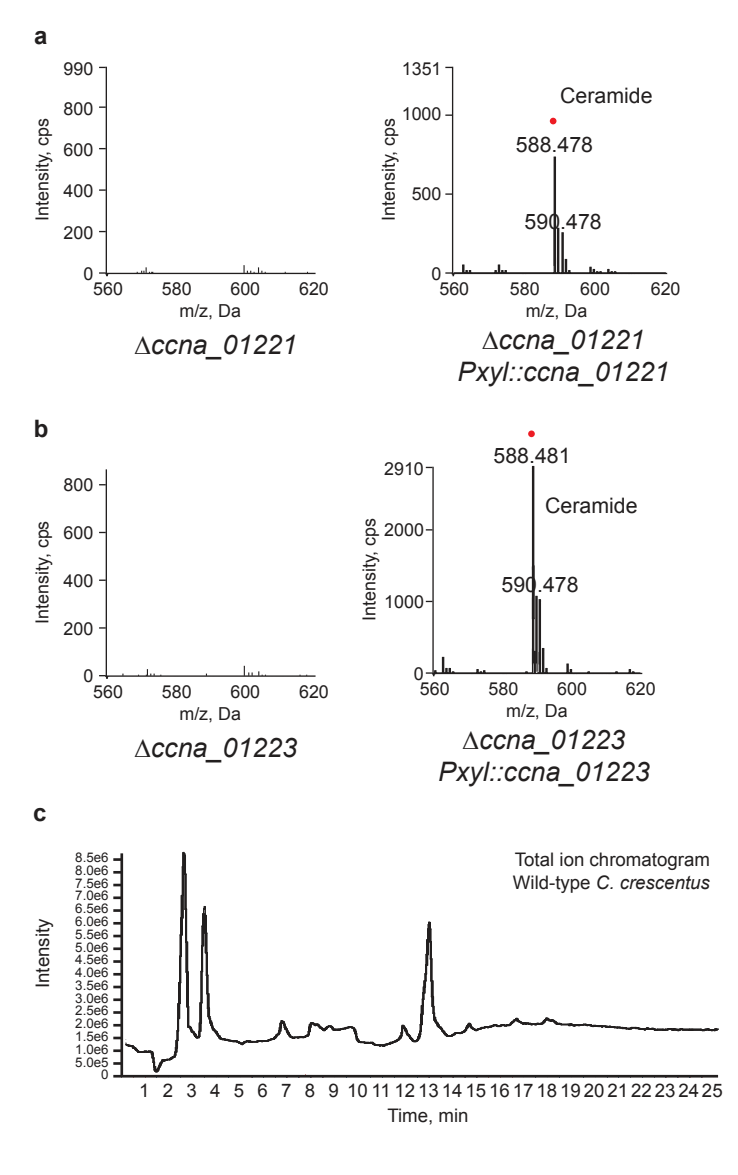


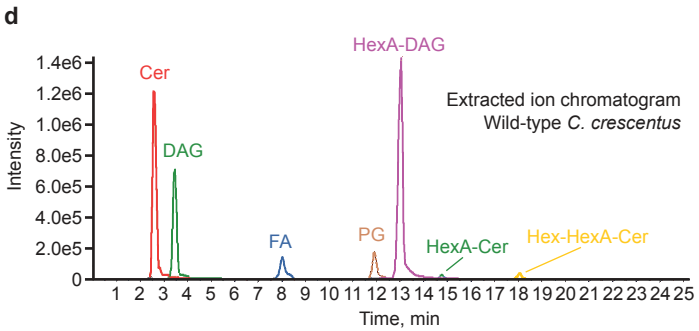


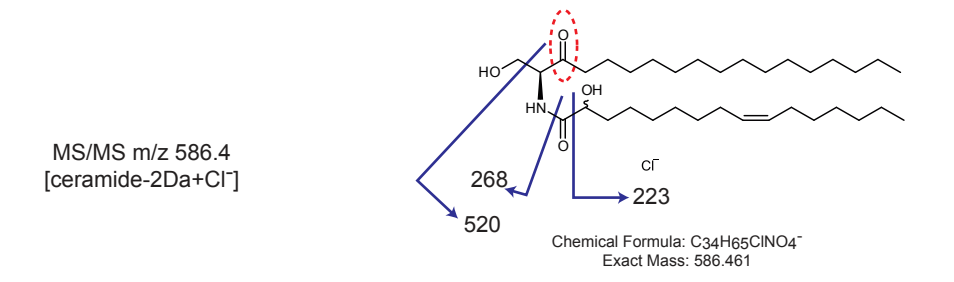
Extended Data Figure 1

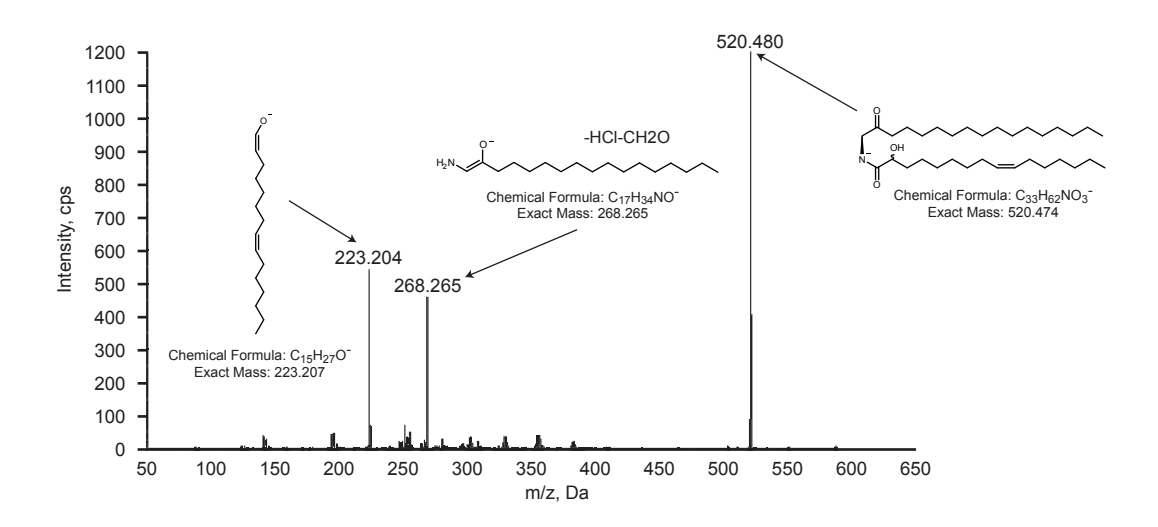


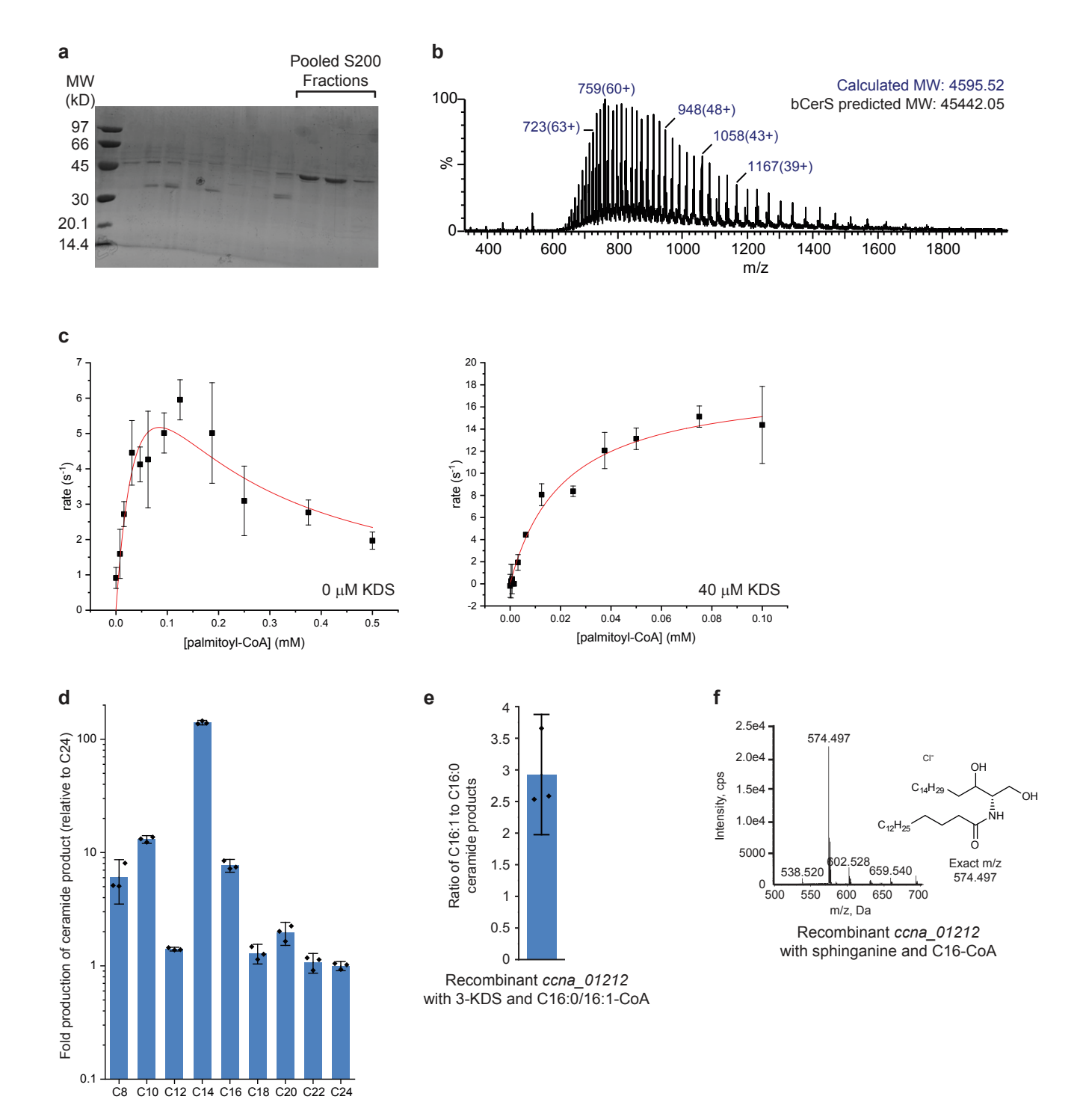


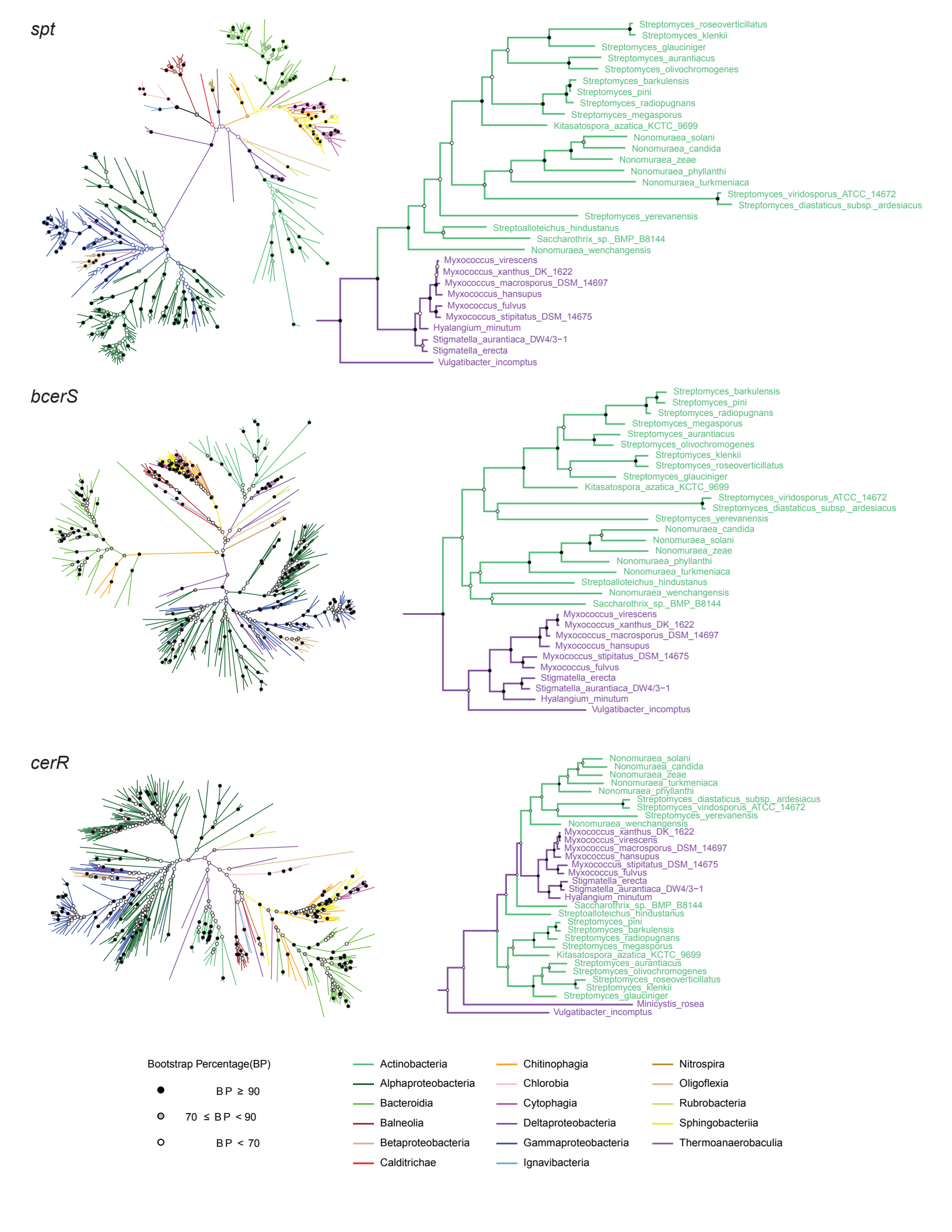




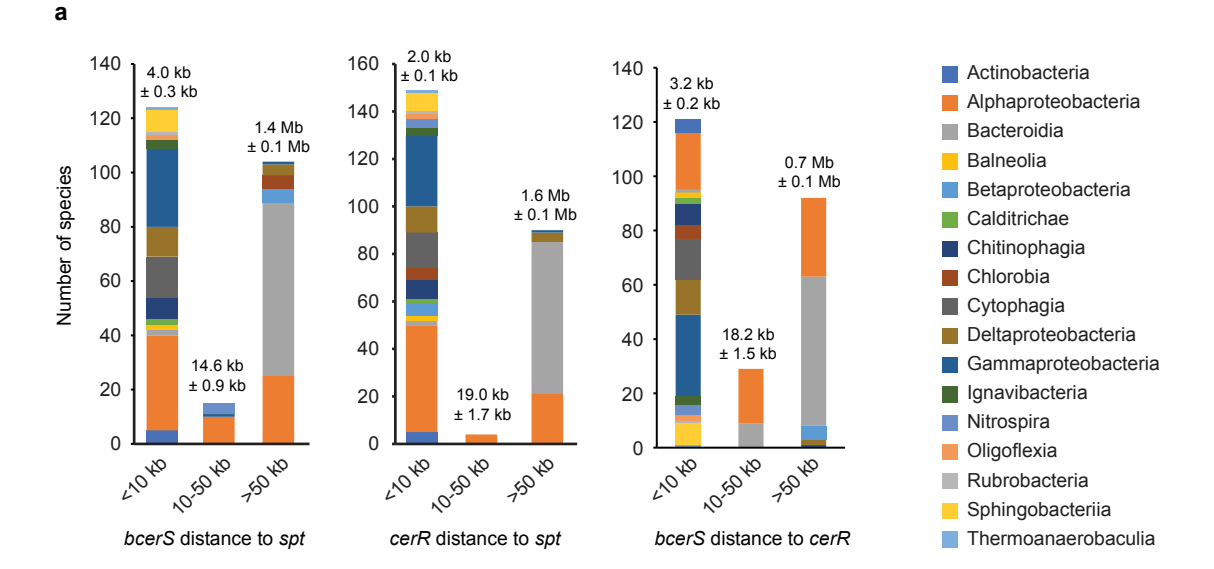


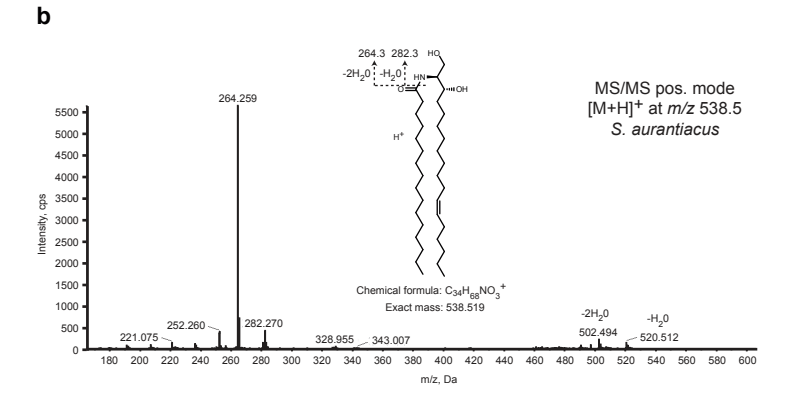


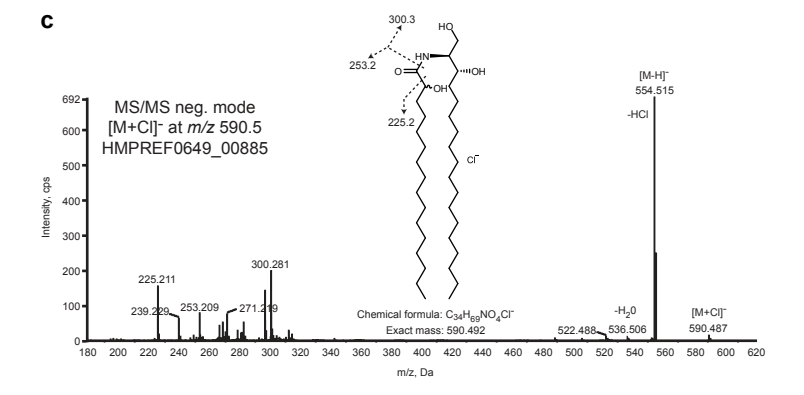


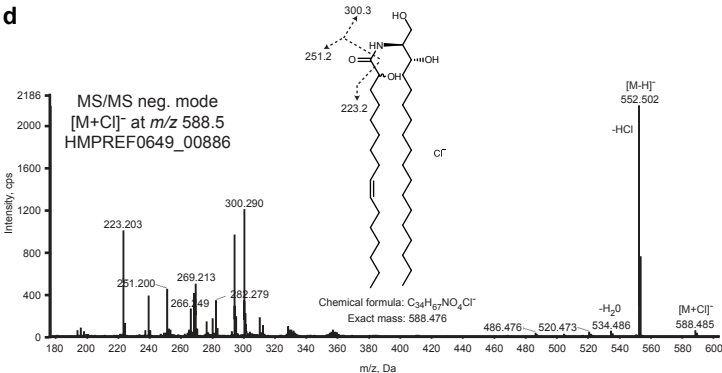


Extended Data Figure 7

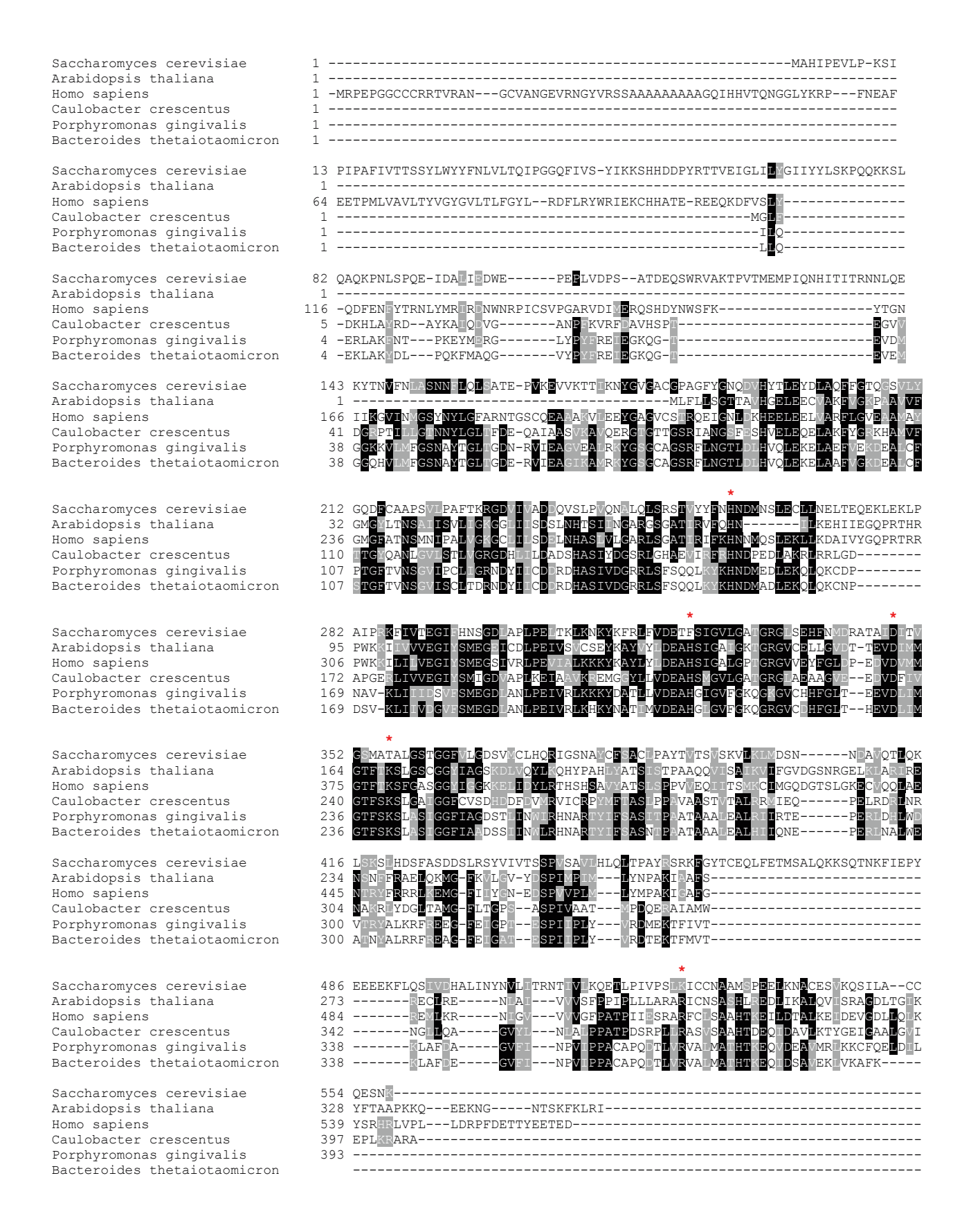




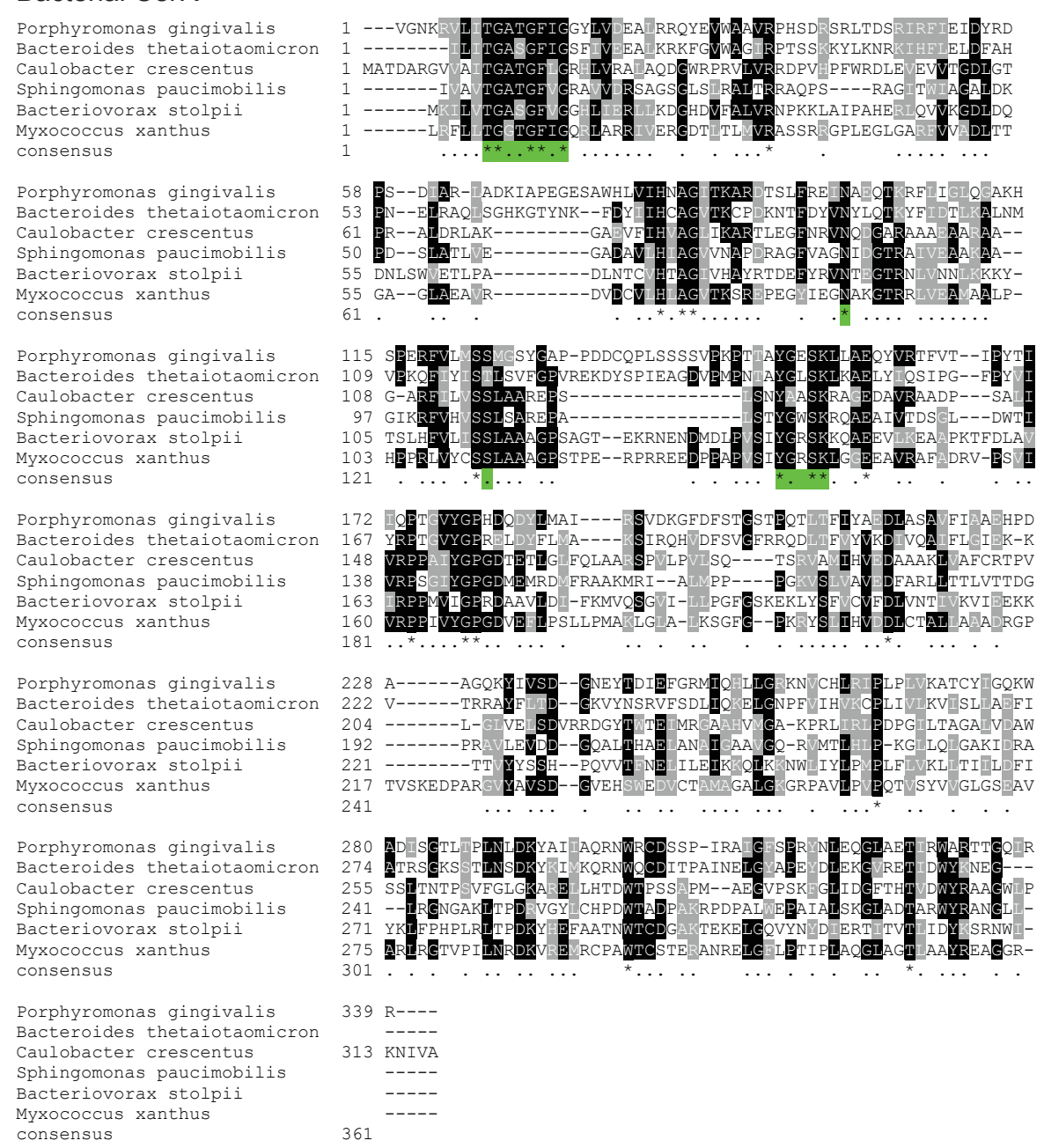




Serine palmitoyltransferase alignment

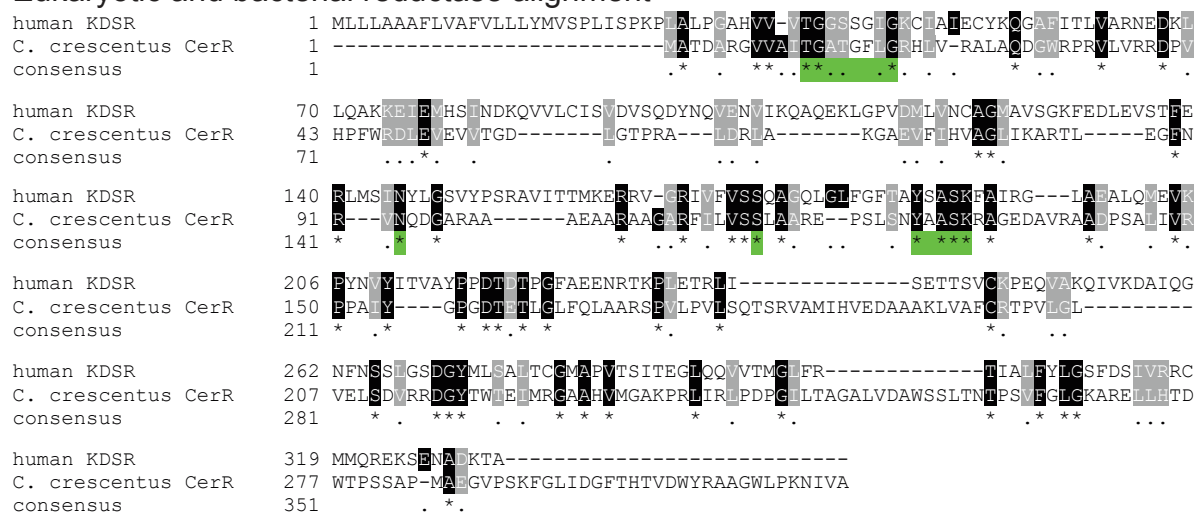


Bacterial CerR



b

Eukaryotic and bacterial reductase alignment



Bacterial bCerS

consensus MDAV-SED Streptomyces aurantiacus 51 HRNPFHTVGTVRLFLARRSGTVIGRIAAIVDPR-----YQERHDLKCGQFGLFEC 61 .. consensus Porphyromonas gingivalis

Bacteroides thetaiotaomicron
Caulobacter crescentus
Sphingomonas paucimobilis
Bacteriovorax stolpii
Myxococcus xanthus
Streptomyces aurantiacus
101 VVDALFHAVSDWARSKGMDMLQGPVGFTDMDHEGMLIDGFDQLGTVATIYNYAYYPKQLE
WSALIKTVEDWGKERGMTHITGPLGFTDFDAEGMLIDGFDQLSTVATIYNHPYYPVHME
103 VFRALIAKAEGWLREQGMTRAVGPFNLSINZBVGLLVWGFDTPPMVLMGHDPVYAGPRVE
104 VFRALIAKAEGWLREQGMTRAVGPVSQSIWZBPGLLVQGFDQDPTIMMGHARPEYQGWLE
105 VAQCLVNVAASELKKKGITSVQGPMNPGTNYECGLLILKYDDAPQIMMTYNPPYYETLFN
106 WARTLIESAATWLRLEGMDAMLGPANLSSNQ WGLLIDGFDTPPAVMMPHNPPYYAALLE
107 STREED STRINGE consensus Porphyromonas gingivalis

161 RLGFIKDQDWKEYKIFV--PTEIPEKHRISEIVRQKYGLKTLKFRTRK-EVMPYAHRIF
Bacteroides thetaiotaomicron
Caulobacter crescentus

169 EQGYAKAQDLFAYKADE--TGDIPEIAQRRVKRGLPS-GVVLRQIDM--SRYDQBVQTLT
Sphingomonas paucimobilis

163 AVGYTTIKQLFTYELDI--TQEFPPIVQRIIKSGEKNERIRVREVNK--AKFEEDAAILL
Bacteriovorax stolpii

164 EMGFFKAMDLLAYNISP--DIKLPQIIVDIAARTEKKSKVTYRTVDL--KNWKKBLEIFF
Myxococcus xanthus

176 ACGLTKAKDLYAYELSS--SAQPPEKVVRIABKIRVRDGVVVRPVNM--KDLABVKRIR
Streptomyces aurantiacus

181 .*.....*....* Porphyromonas gingivalis

Bacteroides thetaiotaomicron
Caulobacter crescentus
Sphingomonas paucimobilis
Bacteriovorax stolpii
Myxococcus xanthus
Streptomyces aurantiacus
Caulobacter
Caul Porphyromonas gingivalis

Bacteroides thetaiotaomicron
Caulobacter crescentus

Sphingomonas paucimobilis
Bacteriovorax stolpii

Bacteriovorax stolpii

Myxococcus xanthus

Streptomyces aurantiacus

330 IP-IFQKNGVEYAESNPELETNMAVOMQWNYFERK-HKTRRAFIKRI

331 IP-VYQKLGFIFAESNPELELNGKVOAQWDYFETKQHKRRRAFIKEI

332 IP-VYQKLGFIFAESNPELELNGKVOAQWDYFETKQHKRRRAFIKEI

333 RD-MAMSLGYNRYEISWVLEANKAMTHIAENVGGT-YKTYRVYEKAL

334 RRASITKYGASROEIGWILDDNQGMRSIAETINSRVNKTYNVYARDL

335 QVSIQQNSRIKNVEISWILETNVEMNKPLIRMSCPAYKRYRIVEKAL

345 LRTAKR-LGYVGGEISWTLEDNHLVNRAIESMGAQRSKTYRVYTRAL

337 QRTAFR-LGYTETECSWILEDNRDANRSTKAIGGIHFRTHRIYERA
238 CRTAFR-LGYTETECSWILEDNRDANRSTKAIGGIHFRTHRIYERA
239 CRTAFR-LGYTETECSWILEDNRDANRSTKAIGGIHFRTHRIYERA-361 consensus

b

Eukaryotic CerS Lag1P conserved domain

S. cerevisiae	222 RKDYKELVFHHIVTLLLIWSSYVFHFTKMGLAIYITMDVSDFFLSLSKTLNY
A. thaliana	128 RSDFGVSMGHHIATLILIVLSYVCSFSRVGSVVLALHDASDVFLEVGKMSKY
H. sapiens	150 RKDSVVMLLHHVVTLILIVSSYAFRYHNVGILVLFLHDISDVQLEFTKINIY
M. musculus	150 RKDSVVMLVHHVVTLLLIASSYAFRYHNVGLLVFFLHDVSDVQLEFTKLNIY
D. rerio	154 RKDSLVMVVHHFITLALITFSYAFRYHNIGILVLFLHDINDVQLEFTKINVY
consensus	241 *.***********

